DYNAMIC SIMULATIONS OF THE IMPACT OF DEPRESSURIZATION OF A VESSEL ON AN INTERCONNECTED VESSEL

A Thesis

by

JASIR JAWAD

Submitted to the Office of Graduate and Professional Studies of
Texas A&M University
in partial fulfillment of the requirements for the degree of

MASTER OF SCIENCE

Chair of Committee,	Luc N. Véchot
Co-Chair of Committee,	Marcelo Castier
Committee Member,	Dominique Guérillot
Head of Department,	M. Nazmul Karim

December 2018

Major Subject: Chemical Engineering

ABSTRACT

Effluent handling systems such as containment vessels along with scrubbers and flare system are used for the storage and treatment of the emergency discharge from the relief system. In case of a runaway reaction or blowdown of a pressure vessel, the relieved stream is usually directly directed to a containment vessel also known as catch-tanks or dump tanks which have several benefits including moderation of the flow for later treatment process and returning the process vessel to service in a shorter time. Many researches have been conducted on the depressurization of a pressure vessel and vent sizing, but only few take into account the impact of depressurization on the catch-tank. The objective of the thesis is to present a dynamic simulator capable of simulating the depressurization of a pressure vessel which is connected and vented to a catch-tank.

To achieve the goals of the study, the capabilities of an existing dynamic simulator for the simulation of venting and leaks from pressure vessels were enhanced. The simulator was limited to the simulation of a single vessel which was extended to the simulation of multiple vessels. A one dimensional transient heat transfer model was included in the simulator assuming the vessel is insulated from outside. Furthermore, an experimental study was conducted by depressurizing non-reacting gases from a pressure vessel to a catch-tank where the pressure and temperature were measured during the process. Moreover, a study of the impact of variation of the parameters such as initial pressure in the vessel, nature of the gas, composition in a mixture of gases and diameter of the tube connecting each vessel is conducted. The experimental data generated from these experiments are used to validate the dynamic simulator, and is presented in the results.

DEDICATION

This thesis is dedicated to my beloved parents, who have been a source of inspiration and taught me and gave me strength, who continually provided me with emotional, moral and financial support.

ACKNOWLEDGEMENTS

I would like to thank my committee chair, Dr. Luc N. Véchot, who has always motivated me and provided support and guidance throughout the course of this research. I would also like to extend my gratitude towards my committee co-chair, Dr. Marcelo Castier, who provided me with the opportunity to work on this thesis, and for giving me his undivided attention, time and expertise to learn and excel at the project. A thanks also goes to Dr. Dominique Guérillot for his collaboration, perspective and serving as an advising committee member. I wish to thank Dr. Rafael de Pelegrini Soares for his contribution by providing his expertise and valuable insights for the project.

I would like to acknowledge and thank Itochu Corporation for supporting my M.S. by providing a fellowship for a year and Mary Kay O'Connor Process Safety Centre Qatar for supporting the rest of the education and research at Texas A&M University at Qatar.

Thanks also go to my friends and colleagues and the department faculty and staff for making my time at Texas A&M University a great experience. Finally, thanks to my parents and brothers for their encouragement, patience and love.

CONTRIBUTORS AND FUNDING SOURCES

This work was supervised by a dissertation committee consisting of Dr. Luc N. Véchot and Dr. Marcelo Castier of the Department of Chemical Engineering and Dr. Dominique Guérillot of Petroleum Engineering. All work for the dissertation was completed independently by the student. Graduate study was supported by an Itochu fellowship from Texas A&M University and funding from Mary Kay O'Connor Process Safety Centre Qatar consortium members for the first and the second year at the university respectively.

NOMENCLATURE

A_{eff}	Effective area of the orifice	m^2
A_{wall}	Area of the vessel wall	m^2
$A_{orifice}$	Area of the discharge orifice	m^2
C_d	Discharge coefficient	
C_p	Specific heat capacity at constant pressure	J/kg.K
$C_{p,steel}$	Heat capacity as a function of temperature	J/kg.K
C_v	Specific heat capacity at constant pressure	J/kg.K
c_{ideal}	Speed of sound in ideal gas	m/s
$D_{cylinder}$	Diameter of a cylindrical vessel	m
D_{eff}	Effective diameter of the orifice	m
$D_{orifice}$	Diameter of the discharge orifice	m
G_c	critical mass flux	$kg/s.m^2$
h	Height of the cylindrical vessel	m
h_{conv}	Heat transfer coefficient	$W/m^2.K$
h_{ex}	Enthalpy per unit mass of exit stream	J/kg
h_{fluid}	enthalpy of the fluid per unit mass	J/kg
h_m^{in}	Molar enthalpy of inlet stream	J/mol
h_m^{out}	Molar enthalpy of outlet	J/mol
k	Isentropic coefficient	
k_s	Thermal conductivity of solid	J/m.s.K

M_{air}	Molar mass of air	kg/mol
M_{helium}	Molar mass of helium	kg/mol
M_m^{in}	Molar mass of inlet stream	kg/mol
M_m^{out}	Molar mass of outlet stream	kg/mol
n	Number of nodes in vessel wall	
n_{ij}	Number of moles of component i in vessel j	mol
$\dot{n}_{im}^{in}$	Molar flowrate of i component in m inlet stream	mol/s
$\dot{n}_{im}^{out}$	Molar flowrate of i component in m outet stream	mol/s
n_{dp}	number of data points	
ns_{in}	Total number of inlet streams	
ns_{out}	Total number of outlet streams	
P	Pressure within the vessel	Pa
P_1	Pressure within vessel 1	Pa
P_2	Pressure within vessel 2	Pa
P_s	Pressure of the stream	Pa
P_2	Pressure in the catch tank	Pa
$\dot{Q}_j$	Heat flow in or from vessel j	J/s
$\dot{R}_{ij}$	Reaction generation or consumption term	mol/s
R	Gas constant	J/mol.K
t	Time	s
T	Temperature of the gas	K
T_0	Temperature of node at outer side of the vessel wall	K

T_1	Temperature of node 1 in the vessel wall	K
T_f	Temperature of the fluid in the vessel wall	K
T_l	Temperature of node l in the vessel wall	K
T_n	Temperature of node at the inner side of the vessel wall	K
T_s	Temperature of the stream	K
T_w	Temperature of the wall	K
u_m^{in}	Velocity of the inlet stream	m/s
u_m^{out}	Velocity of the outlet stream	m/s
U_j	Total internal energy of fluid and the vessel	J
U_s	Internal energy of the solid	J
U_{s0}	Internal energy for node at outer side of the vessel wall	J
U_{sl}	Internal energy for node l of the vessel wall	J
U_{sn}	Internal energy for node at inner side of the vessel wall	J
$U_{f,j}$	Internal energy of the fluid in vessel j	J
V_s	Volume of the solid in vessel	m^3
V_{s0}	Volume for the node at outer side in vessel wall	m^3
V_{sl}	Volume of the element for node l in vessel wall	m^3
v	Molar volume	m^3/mol
v_{ex}	Specific volume of exit stream	m^3/kg
v_s	Molar volume of the stream	m^3/mol
w	Thickness of the vessel	m
x	Distance from outer wall of the vessel	m

Δx	Distance between the nodes in the vessel wall	m

Other symbols

γ	Ideal gas specific heat ratio	
ρ	Density of the fluid	kg/m^3

TABLE OF CONTENTS

Page

Page

LIST OF FIGURES

Page

Page

Page

LIST OF TABLES

Page

Page

1. INTRODUCTION

Thermal runaway in reactors and storage vessels has contributed to major incidents in the past such as the Seveso and Bhopal disasters. Exothermic reactions such as the decomposition of organic peroxides may trigger a runaway reaction as they undergo self-heating. The phenomenon occurs when the heat generated in a reaction vessel becomes higher than the heat removed by cooling system. The excessive heat generated results in the increase of temperature inside the vessel and therefore, the increase in reaction rate as per the rule of thumb which states that for every 10 °C rise in temperature the reaction rate doubles. The continuous increase in the generated heat and the reaction rate leads to exponential rise of temperature and causes overpressure in the vessel as a result of violent boiling and rapid gas generation. Due to this sudden and exponential increase in pressure, it may easily exceed the maximum allowable working pressure of the vessel, hence, leading to the rupture or explosion of the pressure vessel, releasing possibly toxic and/or flammable chemicals into the environment.

The main causes for the incidents involving runaway reactions have been identified as an inadequate understanding of the reaction chemistry, operational procedures and training, engineering design for heat transfer and control and safety back-up systems [1]. The last line of defense against the disastrous consequences are the emergency relief systems which activate automatically when the pressure inside the vessel exceeds the threshold value. The vessel is depressurized and protected by venting through either a pressure relief valve or bursting disc. The hazardous material discharge to atmosphere is contained or reduced by employing effluent handling systems which consist of containment systems such as catch-tanks or dump tanks,

vapor/liquid separators, gas scrubbers and flares. Industries use catch-tanks to receive the emergency discharge directly from the reaction vessel and contain any vapor or liquid that can be fed to a scrubber or flare for further treatment at a lower and controlled flowrate [2]. Using catch-tanks with the relief system prevents the discharge of liquid and solids into the vent header system, moderates the gas and vapor load in the vent system and allows the process vessel to return to service in a shorter time [3].

There are models and commercial simulators available in literature to simulate venting from a vessel which undergoes a runaway reaction, but there is a lack of a simulator capable of predicting thermodynamic properties during a depressurization process from vessel which is vented to a catch-tank. Therefore, in this work, an extended version of an existing dynamic simulator [4, 5] is presented, capable of simulating the depressurization of a vessel by venting the stream to a catch-tank. The work also includes depressurization experiments conducted using air, nitrogen and helium pressurized in a vessel and released into another vessel by opening of a valve. The experimental study also investigates the impact of factors such as initial pressures in depressurized process vessels, nature of gas, composition in a mixture of gases and diameter of the tube connecting the vessel and the catch-tank. The experimental data generated is also used to validate the extended simulator.

The next chapter presents a review of different experiments and simulations conducted on the depressurization of vessels in the past, and also the development of the dynamic simulator used in this study. This is followed by chapter 3, which gives an overview of the scope of work. The methodology is described in chapter 4, which discusses the details of the extension conducted on

the dynamic simulator, including the simulation of multiple vessels and the addition of a heat transfer model. Moreover, the experimental setup, procedures, and experiment matrix are also given in the final section of this chapter. Then, chapter 5 discusses the results from both the experiments and the simulations, along with their validation. The thesis ends with a chapter dedicated to the conclusions and suggestions for future work.

2. LITERATURE REVIEW

This chapter presents the literature on different experiments and simulations conducted for studying depressurization of a pressure vessel. It mainly discusses the depressurization of vessels involving non-reactive gases. Moreover, some literature for runaway reaction cases have also been included, for cases in which the experiments and simulation included the use of catch-tank. A review of dynamic models and heat transfer models in the literature on the depressurization process is mentioned.

2.1 Fluid flow models

The prediction of flowrate is an important factor in the depressurization process to efficiently design the pressure relief systems. The depressurization is a dynamic problem, and since the flowrate depends on the conditions of the tank being depressurized which changes throughout the process and outlet conditions, it is essential to predict the varying flowrate from the depressurized vessel using fluid flow models. Some of the models used to predict the flowrate from a depressurizing vessel have been discussed in this section.

Crowl and Louvar [6] present a method for the calculation of the flow of ideal gas through holes assuming that the release is free expansion where the frictional resistance is low and kinetic energy is high for which the assumption of isentropic behavior is usually valid [7]. Under the assumptions of negligible potential energy changes and no shaft work, the velocity of the gas flowing from the orifice is calculated from the energy balance which is then used to calculate the molar flowrate.

However, non-ideality of the gas is not considered and the heat capacities used for the calculation are constant. For a single phase flow of gas through the hole, critical mass flux is given by Equation (1):

$$G_c = \left(\frac{2}{\gamma + 1}\right)^{\frac{\gamma+1}{2(\gamma-1)}} \sqrt{\gamma P \rho} \tag{1}$$

where G_c is the critical mass flux, γ refers to the ratio of specific heat capacities of ideal gas or isentropic expansion coefficient, P and ρ denotes the upstream pressure and density of the gas.

Lenclud and Venart [8] assume that flow is choked during the whole process of depressurization and calculate the critical mass flux for a perfect gas and isentropic conditions using Equation (1). Similarly, Woodward and Mudan [9] use the same technique for calculating the discharge rate of the gases. The API 520 also recommends this method for evaluating the discharge rate for ideal gases for critical and sub-critical flow [10]. However, API suggests not using the real gas heat capacities ratio as it does not provide a good representation of an isentropic expansion coefficient. Instead, for a real gas the Equation (2) is used to determine the isentropic coefficient [10].

$$k = -\frac{v}{P} \times \left(\frac{\partial P}{\partial v}\right)_T \times \frac{C_p}{C_v} \tag{2}$$

where v, P and T are the molar volume, pressure and temperature of the gas. C_p and C_v refers to the heat capacity at constant pressure and volume respectively. The mass flux for a critical flow is given by Equation (1), replacing γ with k obtained from Equation (2).

Leung and Epstein [11] criticized the modifications to ideal gas flow equations involving the use of compressibility factor which lead to inaccurate results when Z deviates considerably from unity. The critical mass flux was given by maximizing Equation (3):

$$G_c = \frac{2}{v_{ex}}(h_{ex} - h_{fluid})^{\frac{1}{2}} \quad (3)$$

Where the v_{ex} and h_{ex} are the specific volume and enthalpy of exit stream respectively. h_{fluid} refers to the enthalpy of the fluid. The method also includes the use of cubic equation of state to account for non-ideality in the fluid behavior, however, the ideal gas heat ratios are used in the calculation for the simplicity of the model.

Leung [12] developed omega method based on homogenous flow model to account for the compressibility of the two-phase mixture. This method has been recommended by API for sizing for the relief valve [10]. Although the method is for two-phase mixture, by setting the omega parameter to $1/\gamma$, the sub-critical and critical mass flux can be evaluated for a non-condensable gas [13]. An extension to omega method is provided by Diener and Schmidt [14] by accounting for boiling delay for two phase flow to calculates flowrate reliably, however for single phase flow omega parameter set to $1/\gamma$ can be used to calculate the flowrate as in omega method. Overall, the single phase models are well established in the literature.

2.2 Depressurization experiments and simulation

Byrnes et al. [15] studied the rapid depressurization from 135 to 13.5 atm of a gas cylinder containing nitrogen and hydrogen gas through experiments and analysis. They conducted multiple

test varying the depressurization rate and found that at a high depressurization rate the heat transfer from the wall did not have appreciable effect on the gas temperature; whereas for a low depressurization rate the drop in gas temperature was small and the temperature started increasing at the end of the experiments due to the heat transfer with the wall. For comparison with the experimental data, the decrease in pressure was given by an exponential function of the time and also the heat transfer from the walls to the gas was assumed to be predominantly by natural convection and predicted by a turbulent free-convection correlation.

Experiments involving the discharge of pressurized nitrogen and helium from a cylindrical vessel through an orifice to the atmosphere were conducted by Landram [16], who also simulated the process to obtain the temperature of the gas within the cylinder assuming ideal gas behavior. He included a quasi-steady free convection model for the wall-gas interface and reported that the fluctuations in the measured temperature during the depressurization of the vessel correspond to development of a thermal diffusion layer on the wall.

Haque et al. [17] studied rapid depressurization from large pressure vessels containing nitrogen gas and multicomponent gas mixtures, which were simulated using a computer package called BLOWDOWN. These experiments indicated that the dominant mode of heat transfer was natural convection. However, the experiments and simulations are limited to single vessel depressurized to ambient pressure. In 1992, Haque et al. [18] provided a complete description of the BLOWDOWN model which uses discrete steps of pressure decrement in the vessel to represent the whole depressurization process instead of time duration for the calculation. Moreover, the model uses an extended principle of corresponding states to predict the thermophysical properties

which is more accurate than cubic equation of state but requires more runtime. The experimental validation of the BLOWDOWN model shows that it predicts the bulk fluid and wall temperatures with a maximum estimated uncertainty of ±3 K and ±5 K [19].

In 1990, a study conducted by Skouloudis et al. [20] showed the difference between the depressurization of a vessel to the atmosphere and to a catch-tank. Experiments included the depressurization of a steam-water mixture and viscous fluid (luviscol solution). The process was simulated using the computer codes SAFIRE [21] and DEERS [22]. The results obtained from both simulators and experiments were compared, including the pressure and mass inside the vessel and the catch tank as a function of time, but not the temperatures in the vessels.

Friedel et al. [23] studied the pressure behavior and mass inside the vessel to assess the fluid dynamic and thermodynamic components of an extended version of the computer program SAFIRE. The experiments included:

(1) a chemically non-reactive refrigerant in a vessel which was depressurized to a catch tank that is open to the atmosphere, and

(2) an esterification reaction carried out in the vessel depressurized to a closed catch tank. The results from the simulation shows that pressure in the vessel is predicted accurately except for the initial phase of depressurization.

However, the mass flux predicted by SAFIRE shows deviations from experimental data. Moreover, the temperature of the fluid is not reported in the paper and the model does not take into account the heat transfer with the vessel walls.

Xia et al. [24] presented a simplified model for the depressurization of gas-filled vessels and compared the results with the experimental data in the literature. The mass flowrate was assumed to be time independent and the fluid properties (except density) and heat transfer coefficient of the wall with the fluid are taken as constant. The model uses the virial equation of state [25] to account for the non-ideality in the fluid behavior. Disagreements between the predicted and measured temperature of the gas can be observed, however, there was good agreement for the pressure behavior of the vessel.

Mahgerefteh and Wong [26] developed a simulator called BLOWSIM that incorporates the cubic equations of state, which is used to simulate the blowdown of hydrocarbon mixtures from vessels at high pressures. The model includes non-equilibrium effects between the phases and the effect of sonic flow at the orifice discharge. The heat transfer model used assumes natural convection with the walls of the vessel and negligible temperature gradient in the walls of the vessels. The results are compared with BLOWDOWN simulations using different equations of state, whose effect is shown to be minimal, and shows good agreement of the predicted pressure and temperature with data published in the literature.

Large scale experimental data on runaway reactions are scarce due to the hazards and cost associated with them. Snee and Cusco [27] conducted experiments on laboratory and pilot scale runaway reactions vessels vented to a catch-tank while studying a reaction inhibition technique as an alternate to emergency relief systems. The results from lab scale experiments are used to develop scale-up procedures for the pilot scale experiments. The researchers predict the lab and

pilot scale temperature and pressure behavior in the process vessels; however, the authors do not report any data associated with the catch-tank.

Berge [28] presented the validation of a computer program called VESSFIRE for the blowdown of a vessel by comparing the results with the experiments conducted by Haque et al. and the simulations from BLOWDOWN [19]. The model is capable of simulating heat transfer from fires onto the vessel as well heat conduction in the vessel walls. The results from VESSFIRE show better agreement with the experimental data than those from BLOWDOWN. Though VESSFIRE is capable of simulating vessel depressurization with flow lines and accounting for complex heat transfer with the vessel walls, however, the applications have been limited to the simulation of single vessels only.

Ranong et al. [29] discuss an approach for determining heat transfer coefficients during a filling process, which is what happens to a vessel at low pressure interconnected to a depressurizing vessel. The work focuses on a vessel filling with hydrogen gas, assuming that forced convection is the dominant mode of heat transfer between the inner walls and the fluid at the beginning, while natural convection dominates by the end of the process. The forced convection coefficient is estimated by generating a statistical velocity distribution on the inner side of the wall using CFD models and assuming that the vessel walls are flat plates.

Winters et al. [30] conducted experiments and analysis on helium gas depressurized from spherical supply vessel to a receiver vessel initially at ambient pressure, interconnected by a tube and a valve between the vessels. The experiments were simulated by the NETFLOW analysis code, which

accounts for the flow in vessels, pipes and through valves and orifices taking into account the possibility of choked and non-choked flows. An experimental technique of transient pressure-volume-temperature (PVT) method is used to determine pressure and mass-averaged temperature measurements in the vessels instead of using thermocouple measurements to measure the temperature transients. A heat transfer model assuming natural convection, adiabatic and isothermal cases, has been analyzed along with a model for the mass transfer between the vessels. The simulations assuming natural convection show good agreement with the experimental data, while the adiabatic and isothermal cases show some deviations. Moreover, the temperature behavior in the receiving vessel is not shown in the study.

VBsim, a simulator developed by D'Alessandro et al. [31], incorporates non-equilibrium effects by introducing a partial phase equilibrium approach. It accounts for external and internal heat transfer to/from the walls of the vessel and the mass transfer that takes place inside the vessel. The validation of the experiments shows deviation in the prediction of wall temperatures.

Fischer and Biswas [32] validated the depressurization model of Aspen HYSYS version 9 with the experiments conducted by Haque et al. on the blowdown pressure vessel. The details of the dynamic model used are not provided. The results show good agreement for the pressure inside the vessel while the temperature profiles of the gas and vessel wall show some disagreements with the experimental data.

Another dynamic blowdown simulator is presented by Kim et al. [33], which accounts for both laminar and turbulent flow within the vessel during its depressurization by using empirical

correlations. The experimental data from the literature is simulated using the Peng-Robinson [34] and Soave-Redlich-Kwong [35] equation of states which do not show significant differences.

A numerical model is presented by Park et al. [36] to simulate the rapid depressurization of vessels accounting for non-equilibrium effects on the different phases. The heat transfer model assumes the combined effect of forced and free convection because, as the temperature and pressure drop in the depressurized vessel, the viscosity becomes significant in the heat transfer mechanism. The results from the simulator are compared with different data available in the literature and show that it is able to predict the vapor, liquid and wall temperatures, and the pressure inside the vessel during its depressurization.

2.3 Dynamic simulator development

The dynamic simulation of the depressurization of a vessel by discharging a non-reacting gas into another tank, called catch-tank, is proposed in this work. The dynamic simulator used in the study has undergone many developments in the past few years.

The development began with a dynamic simulator for flash drums proposed by Goncalves et al. [37]. Under the assumption of instantaneous equilibrium, the state of the fluid inside the vessel is determined by solving a flash problem at given values of internal energy, volume and number of moles of the components. To this end, a new algorithm for flash calculation that maximizes the entropy of the system was proposed by Castier [38] and added to the flash drum simulator [39]. Another addition to the simulator was the flash calculations using stagnation enthalpy, specified

entropy and component amounts in a single loop approach for faster calculations and also, an algorithm for sound speed calculations was introduced to determine the exit flow conditions (choked or non-choked) [40]. A simulator for venting and leaks from a single pressure vessel with the incorporating algorithms for phase equilibrium and sound speed in calculation in multiphase was developed by Castier and the group [4, 5], and validated against experimental and literature data. Moreover, the contribution from vessel mass and its construction material in the total internal energy of the vessel was also included in the latest version of the simulator. However, an isothermal approach was used in which the vessel wall temperature was set to the fluid temperature at each time-step resulting in an instantaneous heat transfer between vessel wall and the fluid inside the vessel [41].

It is found that most of the models used as a standard for relief valve sizing and flow through a nozzle does not account for non-ideality of the fluid in their calculations for the prediction of molar flowrate such as API RP 520 for a single phase flow [10]. According to Selmer-Olsen [42], the API recommendation could yield unsafe relief sizing. Most of the experiments conducted and validated in the literature consist of releases from a single vessel to the atmosphere in which case the back pressure does not change. There are few depressurization experiments conducted using catch-tanks but they fail to report all the conditions (temperature, pressure and mass) in each tank as a function of time [20, 23, 27], which motivated the experimental study done in this work.

No specific model or dynamic simulator has been applied to study the behavior of interconnected vessels with emphasis on the impact of depressurization of the process vessel on the catch-tank. Moreover, the literature shows the importance of the heat transfer between the fluid and the vessel

walls during depressurization. Therefore, an existing simulator is extended to simulate interconnected vessels and incorporate the effect of heat transfer between the fluid and the vessel walls in each vessel. The simulator uses rigorous thermodynamic calculations to predict the flow from the vessel assuming an isentropic hypothetical converging nozzle while accounting for non-ideality of fluid behavior and calculates the temperature, pressure and amount of fluid in each vessel as a function of time.

3. SCOPE OF WORK

An uncontrolled exothermic reaction may lead to thermal runaway in the process vessel containing a reaction mixture. As a result, the temperature and pressure exponentially increase, which may lead to catastrophic consequences such as explosion of the vessel. To avoid the consequences in case of such an event, emergency relief systems are used to depressurize and protect the reaction vessel or the storage tank. The relieved stream is then carried to effluent handling systems such as a catch-tank which receives the emergency discharge from the relief devices, which may consist of entrained solids and reaction mass along with the vapor discharge.

Few models and simulators exist to predict the impact of depressurization of a vessel undergoing runaway reaction beyond the venting from the process vessel. Therefore, this thesis aims to develop a simulator for a process consisting of a vessel undergoing depressurization interconnected to a catch-tank which receives the discharge from the vessel. The work in this thesis is limited to experiments and simulations conducted on non-reactive gases depressurized from the vessel. The flow occurs between the two tanks because of the pressure difference. In the simulations, the conditions in each vessel, such as number of phases, temperature, pressure, number of moles and compositions, are predicted as a function of time. The methodology has been divided into two parts:

1. Extending the capabilities of an already existing dynamic simulator for leaks and venting proposed by Kanes et al. through addition of an algorithm for simulation of multiple vessels as the simulator was limited to simulation of one vessel only [4].

Furthermore, heat transfer with the walls of the vessel during depressurization process plays an important role. Therefore, a one dimensional transient heat transfer model was added to the simulator to predict the wall temperatures during depressurization and its impact on the fluid temperature at each time-step. This effect was also incorporated in the catch-tank, whose pressure increases. Moreover, the effect of discharge coefficient is also incorporated to the existing simulator.

2. A study of an inert gas depressurized from one vessel to another was conducted through experimentations. Air, Nitrogen, Helium and a mixture of these gases at different compositions were used in the experiments. The data generated from the experiments was to use to validate the simulator for a non-reactive depressurization process in a closed system of interconnected vessels. Along with the validation, the impact of different initial pressures, nature of gases, composition of mixture and different tube (connecting the two vessels) dimensions on the depressurization process was studied.

The availability of this kind of a simulator allows for the calculation and prediction necessary for not only the vent sizing but the sizing of the catch-tank as well. It gives a complete picture for the vented stream in a process involving the use of catch-tanks which can be used to improve the existing designs of pressure relief systems.

4. METHODOLOGY

It has been seen from the literature that very few models exist that can simulate the behavior of a catch-tank connected to a process vessel during the depressurization process. Since catch-tanks and dump tanks are widely used in industries, it is important to predict the impact of emergency relief from a reaction vessel or a pressurized gas vessel on the vessel itself and the interconnected catch-tanks in the process. As it has been seen from the experiments and simulation, depressurization can result in low temperatures in the tank whereas the filling of the catch-tank increases its pressure and temperature. With this motivation, a dynamic simulator is presented in this work, which is capable of predicting such behavior in interconnected vessels. Moreover, an experimental non-reacting gas depressurization study has been conducted focusing on different parameters that impact depressurization. Lastly, the data collected from experiments is used to validate the extended simulator presented in this thesis.

The methodology is divided into two parts:

1) Extension of the dynamic simulator
2) Experiments for validation of the extended simulator

The rest of this chapter will describe how each phase in the project was carried out.

4.1 Extension of the dynamic simulator

The simulator presented by Kanes et al. [4] and Castier et al. [5] uses a rigorous thermodynamic approach to predict the state of the fluid in the vessel using flash calculations for specified values

of internal energy, volume and number of moles for a multiphase system. The non-ideality is accounted for using the Peng-Robinson equation of state [34]. It is able to simulate multiple leak points from the vessel along with venting from a pressure relief valve during the depressurization of the vessel in case of a runaway reaction. The user can select one of the following different vessel geometries:

1) Vertical cylinder
2) Horizontal cylinder
3) Spherical
4) Horizontal cylinder with hemispherical cap

The output flow is assumed to be through an adiabatic converging nozzle that operates isentropically although the user is able to choose either rectangular or circular orifice geometry. The simulator determines whether the flow will be choked or non-choked based on the sound speed calculations.

4.1.1 Dynamic Simulator EMSO

At first, a dynamic simulator called EMSO (Environment for Modelling, Simulation and Optimisation) [43] was considered for the task of simulation of multiple vessels during a depressurization process. EMSO is a modelling, simulation and optimization environment capable of solving differential-algebraic equations. It includes model libraries for thermodynamic and

process engineering applications along with a thermodynamic plugin for the selection of different equations of state.

Initials runs on EMSO for depressurization of vessel filled with air were successfully simulated. One of the major issues faced was the lack of a sound speed calculation algorithm in EMSO. The proposed solutions included the coupling of EMSO and the dynamic simulator of Kanes et al. [4] in which the thermodynamic calculations would be performed by the latter while EMSO would use its powerful integrator to integrate the differential equations that result from the modeling with multiple interconnected vessels. Another solution was to write a thermodynamic plugin for EMSO to suit the needs of the simulation. Ultimately, both solutions were rejected as extensive time-consuming modifications of the software would have been required. Hence, the simulator proposed by the Kanes et al. was extended as it had all the thermodynamic algorithms necessary to simulate the depressurization process. EMSO has been used to validate the early results from the extended dynamic simulator, which will be presented later in the chapter.

4.1.2 Extension of the Simulator

The dynamic simulator was limited to the simulation of a single vessel and therefore an extension was required to be able to simulate a process vessel and a catch-tank. Figure 1 shows the difference between the previous version of the simulator (left) and the extended version (right).

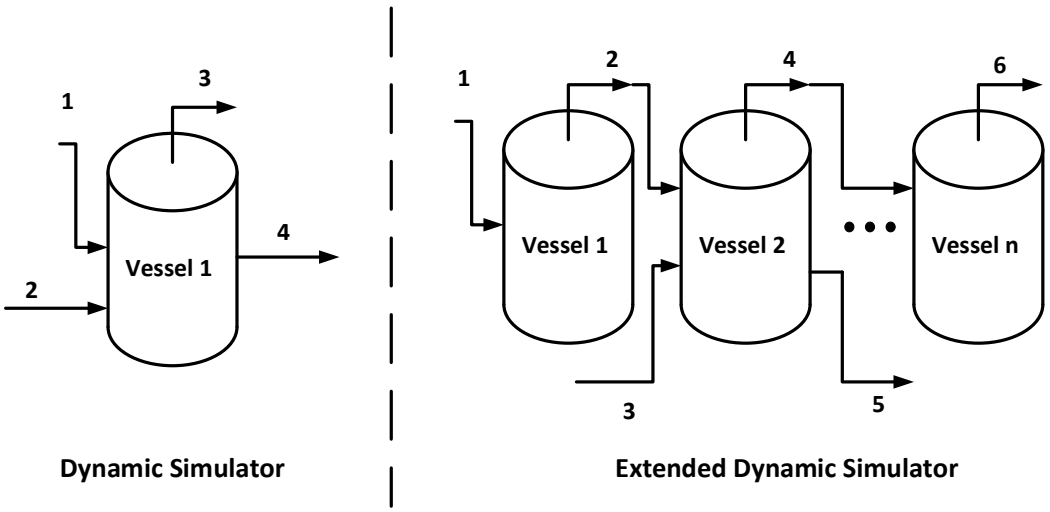

Figure 1. Comparison between the extended and previous versions of the dynamic simulator

It can be seen that the simulator was already capable of handling multiple inlet and outlet streams, whereas the extension provides the connectivity vessels in any order.

The extension was achieved by introducing user-defined stream numbers in the simulator, which can be linked to any of the inlet or outlet of any vessel. Using an indirect indexing technique, the relationship between the flow stream and vessel was established. The existing simulator was only capable of storing information of a single vessel such as dimensions and the initial conditions of the fluid inside the vessel. Its extension enabled the storing and processing of this information for multiple vessel configurations. The extension permits the generation of ordinary differential equations for the mass and energy balance for each vessel in the process simulated along with differential equations associated with heat transfer through the walls of each vessel. The simulation ends when the mechanical equilibrium is reached between connected vessels. A flowchart in Figure 2 provides a summary of the extension algorithm.

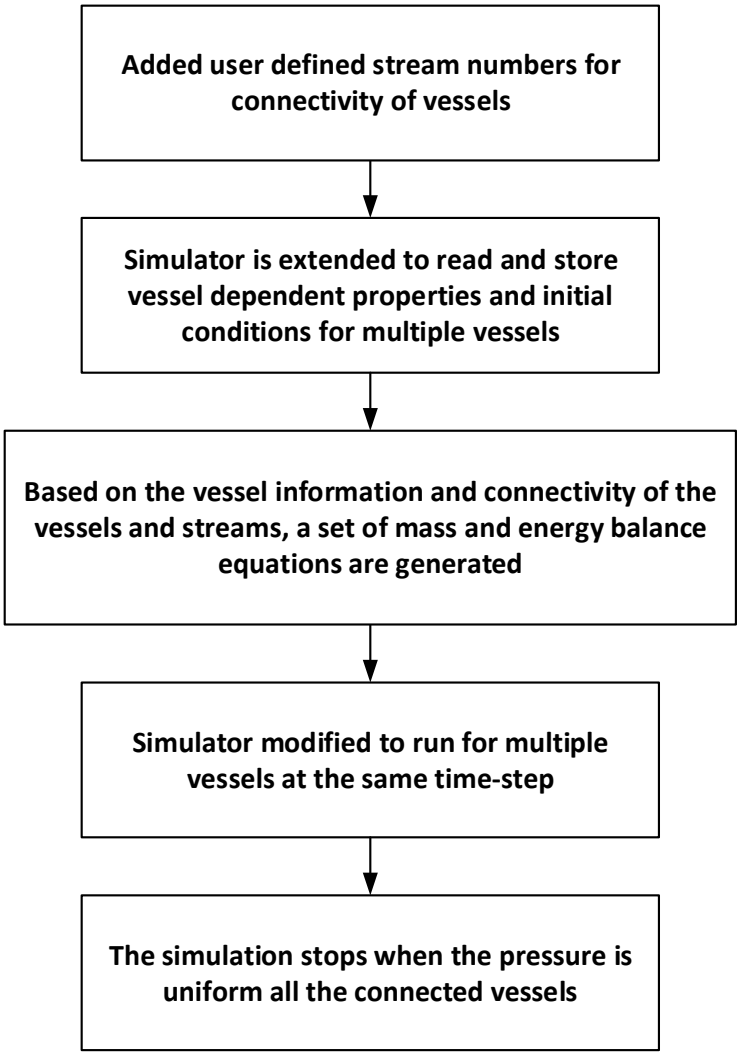

Figure 2. Simulator extension algorithm for handling multiple vessels

4.1.2.1 Mass and Energy Balances

The mathematical model implemented in the simulator consists of a set of ordinary differential and algebraic equations for the mass and energy balances on the vessel and calculation of fluid conditions inside the vessel, along with the prediction of the molar flow from the vessel. Following Kanes et al. [4], the mass balances are given as:

$$\frac{dn_{ij}}{dt} = \sum_{m=1}^{ns_{in},j} \dot{n}_{imj}^{in} - \sum_{m=1}^{ns_{out},j} \dot{n}_{imj}^{out} + \dot{R}_{ij} \quad (4)$$

where t denotes time, n_{ij} and $\dot{R}_{ij}$ refer to the number of moles of component i in vessel j and generation term for component i in vessel j , respectively. The symbols ns_{in}, j and ns_{out}, j are the total number of inlet and outlet streams in vessel j, $\dot{n}_{imj}^{in}$ and $\dot{n}_{imj}^{out}$ are the molar flowrates of component i in inlet stream and outlet stream m , respectively. For the simulation of non-reactive system, $\dot{R}_{ij}$ is zero. The energy balance is:

$$\frac{dU_j}{dt} = \sum_{m=1}^{ns_{in},j} \dot{n}_{jm}^{in} \left\{ h_{jm}^{in} + M_{jm}^{in} \frac{\left(u_{jm}^{in}\right)^2}{2} \right\} - \sum_{m=1}^{ns_{out},j} \dot{n}_{jm}^{out} \left\{ h_{jm}^{out} + M_{jm}^{out} \frac{\left(u_{jm}^{out}\right)^2}{2} \right\} + \dot{Q}_j \quad (5)$$

where U_j and $\dot{Q}_j$ refer to the total internal energy of the fluid in the vessel and heat flow in vessel j respectively. The symbols h_{jm}^{in} and h_{jm}^{out} are the molar enthalpy of inlet and outlet stream, M_{jm}^{in} and M_{jm}^{out} denote the molar mass of each inlet and outlet stream, u_{jm}^{in} and u_{jm}^{out} represent the velocity of each inlet and outlet stream. For the simulation of adiabatic vessels (insulated), $\dot{Q}_j$ is equal to zero.

The differential equations are generated on the basis of information provided to the simulator regarding the number of components, number of vessels and connectivity between the vessels which is then solved by the simulator's integrator at each time-step.

4.1.2.2 Addition of a heat transfer model

A one-dimensional transient heat transfer model has been added to the simulator as a part of its extension. It is known from the literature that heat transfer with the walls of the vessel plays a vital role in determining the temperature of the fluid inside vessel that undergoes depressurization.

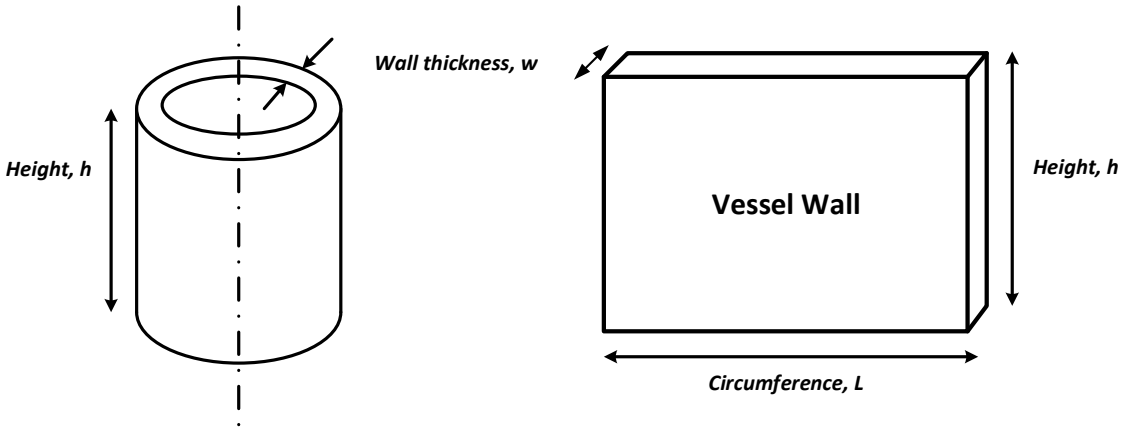

Figure 3. Schematic of heat transfer area in the vessel wall

For this purpose, we start by applying the energy balance on the vessel walls, which are assumed to be a vertical flat plat, as shown in Figure 3. This yields the following equation [44]:

$$\frac{\partial U_s}{\partial t} = V_s k_s \frac{\partial^2 T_w}{\partial x^2} \tag{6}$$

where V_s is the volume of the vessel wall, U_s is the total internal energy of the wall, and k_s is the isotropic thermal conductivity of the solid, assumed to be a constant. The symbol T_w refers to the wall temperature while x is the length from outer side of the vessel wall to inner side.

The boundary conditions associated with Equation (6) are as follows:

1) Outer wall exposed to the atmosphere is assumed to be insulated;

2) Inner wall exposed to the fluid in the vessel has a convective boundary condition.

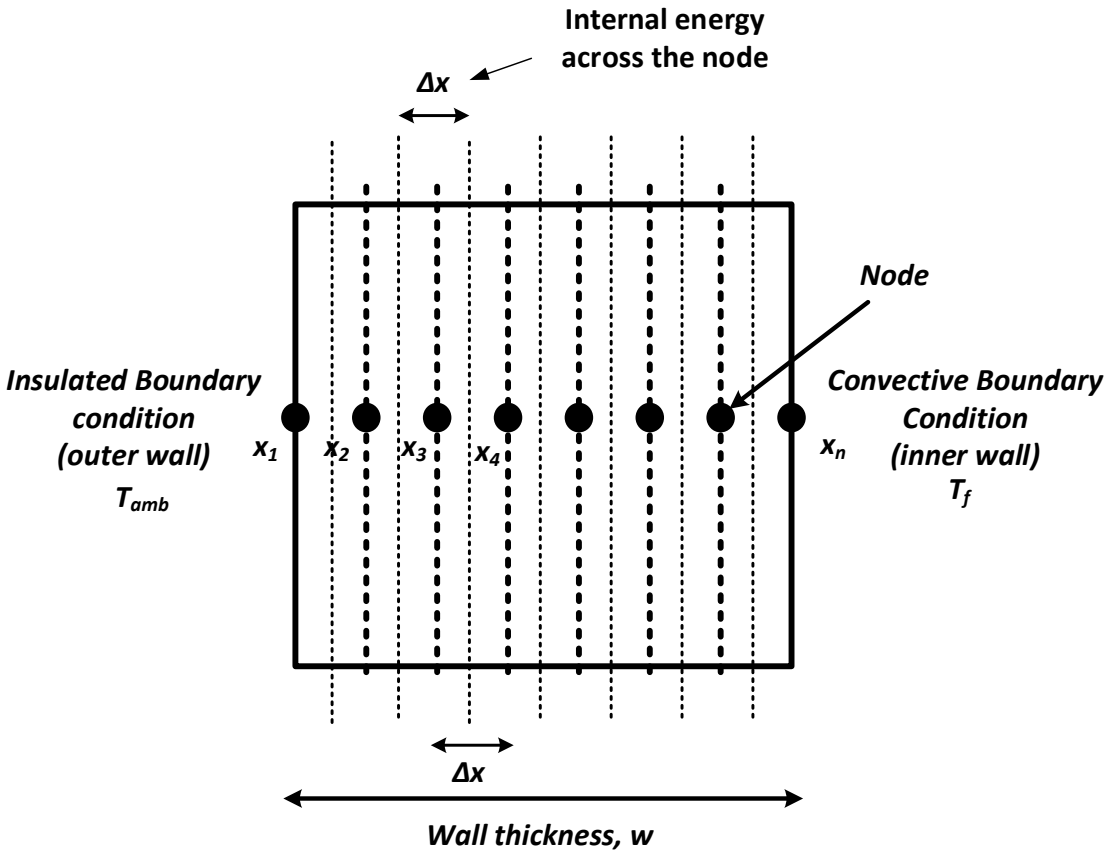

Figure 4. Boundary conditions in the vessel wall

The right hand side of Equation (6) is approximated by finite differences to convert the partial differential equation into a set of ordinary differential equations, which can be solved by the simulator's integrator. In Figure 4, the black dots represent the nodes, which are equally spaced.

$$\Delta x = \frac{w}{n-1} \tag{7}$$

where w is the wall thickness of the vessel and n is the total number of nodes.

The top and bottom parts of the vessel are accounted for in the heat transfer model by assuming the thickness of top and bottom part is same as the thickness of the vessel walls, which is added to the total area, as shown in Equation (8).

$$A_{wall} = \pi D_{cylinder} h + \frac{1}{2}\pi D_{cylinder}^2 \tag{8}$$

where $D_{cylinder}$ and h are the diameter and height of the vertical cylinder, respectively.

4.1.2.2.1 Finite Difference approximation at node=0 (outer wall)

Equation (6) applied at the node at x_0 is approximated by the central difference method. A fictional node at x_{-1} is assumed, as shown in Figure 5.

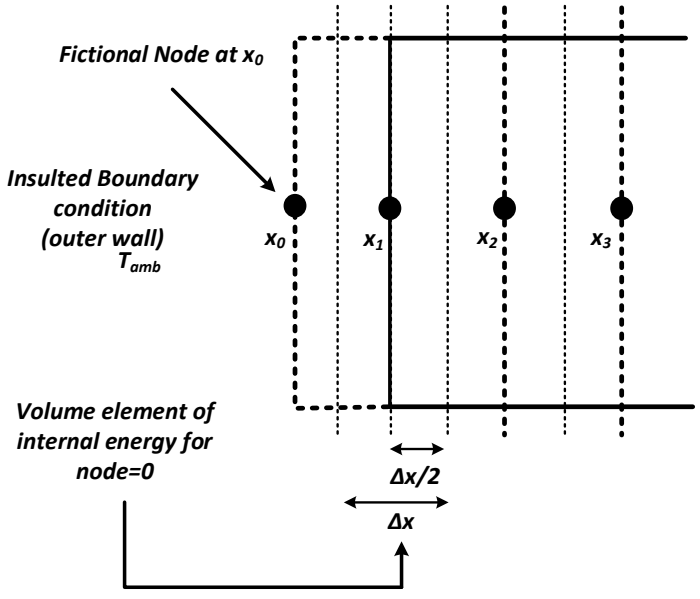

Figure 5. Insulated boundary condition on the outer wall of the vessel

The fictional node temperature T_0 at x_0 is set equal to node temperature T_2 at the x_2 which results in the temperature gradient to be zero at x_1 making the node insulated [45]. Using this approximation, Equation (6) becomes,

$$\frac{dU_{s1}}{dt} = V_{s1}k_s\frac{(2T_2 - 2T_1)}{\Delta x} \tag{9}$$

$$V_{s1} = A_{wall}\frac{\Delta x}{2} \tag{10}$$

4.1.2.2.2 Finite Difference approximation at central nodes ($\mathbf{1 < l < n}$)

Applying central difference approximation to Equation (6) for the inner nodes, the equation becomes:

$$\frac{dU_{sl}}{dt} = V_{sl}k_s\frac{(T_{l+1} + T_{l-1} - 2T_l)}{\Delta x^2} \tag{11}$$

where l is the node's number. The volume of the element is given by:

$$V_{sl} = A_{wall}\Delta x \tag{12}$$

4.1.2.2.3 Finite Difference approximation at node = n (inner wall)

At the inner wall, a convective boundary condition is applied to calculate the heat transfer of the wall with the fluid in the vessel. Therefore, the energy balance for node n, at the inner wall, includes terms from conduction and convection in the wall and is given by the following equation:

$$\frac{dU_{sn}}{dt} = k_s A_{wall}\frac{\mathrm{d}T}{\mathrm{d}x} - h_{conv}A_{wall}(T_n - T_f) \tag{13}$$

Then applying the backward difference method on equation (13):

$$\frac{dU_{sn}}{dt} = k_s A_{wall} \frac{(T_n - T_{n-1})}{\Delta x} - h_{conv} A_{wall} (T_n - T_f) \quad (14)$$

where T_n and T_f are the wall and fluid temperature respectively. The symbol h_{conv} refers to the convective heat transfer coefficient, for which there are prediction methods in the literature However, in this study, the convective heat transfer coefficient will not be calculated; instead, a typical value will be used. The typical value of heat transfer coefficient for gases lies in an approximate range of 25 to 250 W/(m^2.K) [46].

The differential equations (9), (11) and (14) are added to the extended version of the simulator and are solved by the simulator's integrator for each vessel along with the mass and energy balances shown in equation (4) and (5). The fluid internal energy $U_{f,j}$ in vessel j is given by:

$$U_{f,j} = U_j - U_{s,j} \quad (15)$$

4.1.2.3 The discharge coefficient

The discharge coefficient is defined as the ratio of the actual to the theoretical discharge through an orifice. For the flow of liquids through sharp-edged orifice, the value of discharge coefficient is 0.61. The coefficient of discharge for gases is a function of the ratio of outlet to stagnation pressure. Therefore, the discharge coefficient varies with the pressure ratios for gases [7].

In this study, the effect of discharge coefficient is taken into account by reducing the orifice diameter, which reduces the flow area as shown in Equation (18).

$$A_{orifice} = \frac{\pi}{4} D_{orifice}^2 \tag{16}$$

$$C_d A_{orifice} = \frac{\pi}{4} D_{eff}^2 \tag{17}$$

where D_{eff} is the effective diameter of the orifice. Dividing Equation (17) by Equation (16), the following relationship is derived:

$$D_{eff} = D_{orifice} \sqrt{C_d} \tag{18}$$

4.1.2.4 Simulator Algorithm

The simulator works on a certain set of assumptions some of which were present in the previous version of the simulator and were carried over to the current version. Moreover, new assumptions made for the simulation of a depressurization of a vessel connected to a catch tank are also included in the list below:

1) The vessels are rigid and their volumes are known;
2) The fluid in each vessel is in phase equilibrium at all times;
3) The region around the venting point in a vessel acts as a hypothetical adiabatic converging nozzle that operates isentropically;
4) The changes in the potential energy of the fluid inside the vessel and in the inlet and outlet streams are negligible;
5) Kinetic energy of the fluid in the vessel is negligible as compared to the kinetic energy of the fluid at the inlet and exit points;
6) The vessels are assumed to have perfect thermal insulation;

7) The heat transfer through the top and bottom part of the vessels with the fluid in the vessel is accounted for in the total area of the vertical flat plate which is assumed to have the same thickness as the side walls of the vessel;
8) The heat transfer is only one dimensional;
9) Thermal conductivity of the vessel is assumed to be isotropic and constant;
10) The simulator does not include a pipe model. The calculation is done assuming the vessels are directly connected.

The simulator algorithm is mainly adopted from the work of Kanes [47] and Basha [48], however the extensions made in this work are highlighted in red in the flowchart shown in Figure 6.

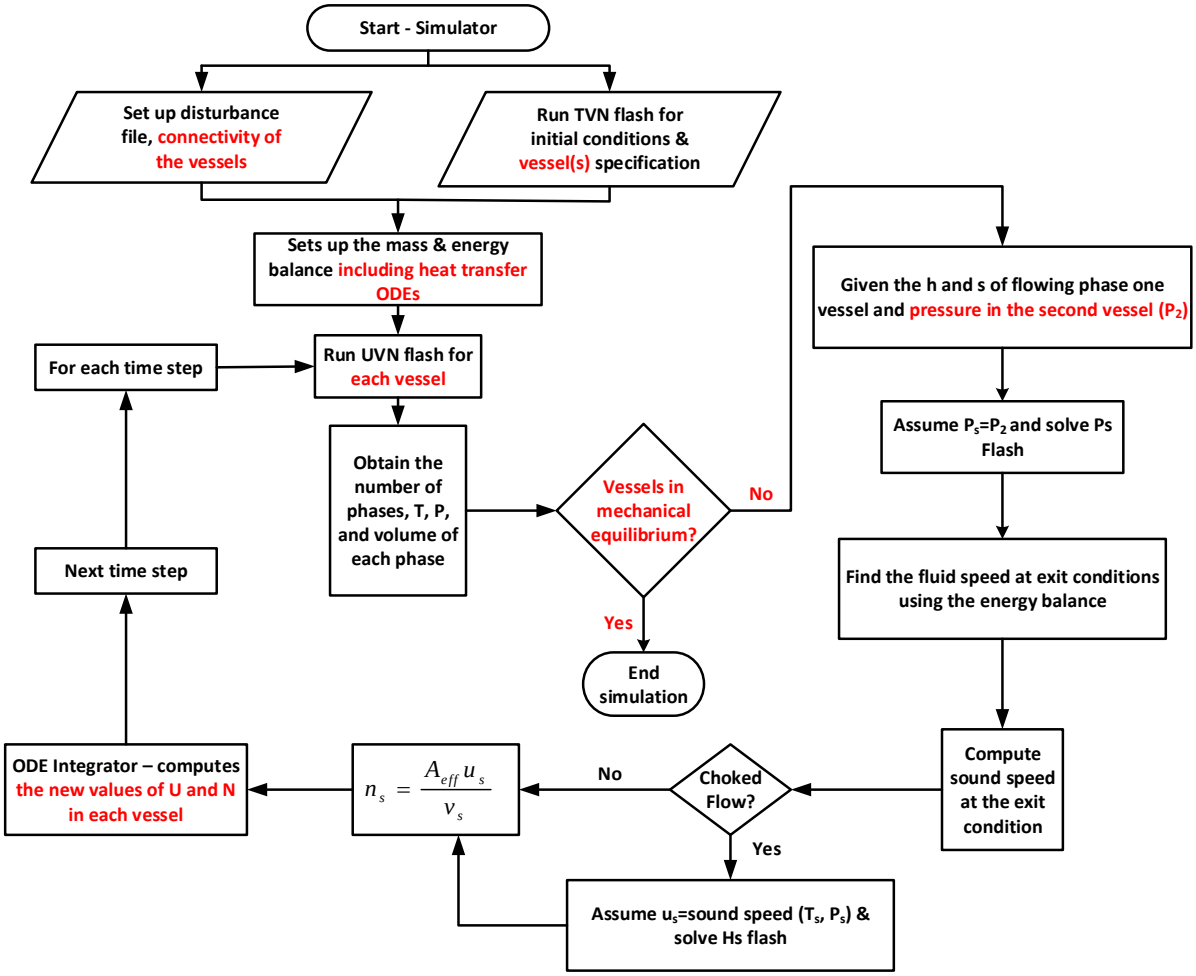

Figure 6. Simulator algorithm with extensions

4.2 Experiments for validation of extended simulator

As there is a lack of study in the literature on the depressurization of a vessel connected to a catch-tank, an experimental study is conducted to understand the behavior of each vessel through the measurement of pressure and temperature during the depressurization. Moreover, factors such as initial pressure, nature of gas, composition in a mixture of gases and the tube dimensions connecting the vessels together are investigated and their impact on the process is studied. The

experimental data generated and analyzed in this regard are then used to validate the results from the simulator.

The following sections will explain the experimental setup and the procedure used to conduct the experiments along with the data correction by applying a first order dynamics to the temperature sensor.

4.2.1 Experimental setup

Phi-TEC II has been used to conduct the depressurization experiments in this study. This equipment is a low thermal inertia adiabatic calorimeter capable of reproducing conditions in large-scale reactors. It enables for the study of vent sizing under runaway conditions and the application of the data generated can be used to determine venting behavior, flow regime, kinetic data, and safe storage and transport of a chemical [49]. Figure 7 shows the schematic of the overall experimental setup while Figure 8 shows the Phi-TEC II containment vessel referred to as vessel 1 in this study, which is primarily used as the depressurized vessel in the experiments.

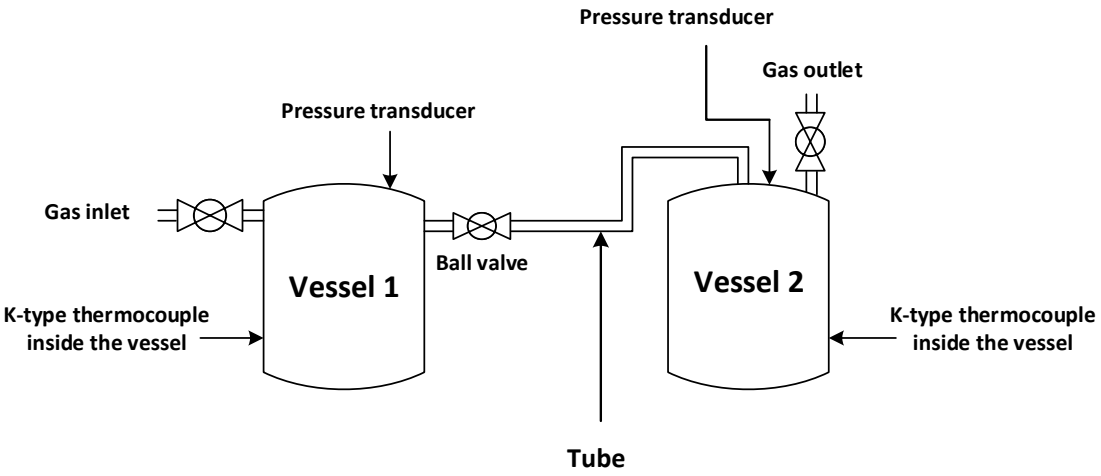

Figure 7. Schematic of overall experimental setup

Figure 8. Phi-TEC II containment vessel/Vessel 1
Reprinted with permission from HEL Ltd [49]

Along with the Phi-TEC II, another pressure vessel (4600 series Parr instrument company reaction vessel), referred to as vessel 2 in this study, is used as catch tank, to receive the discharge from vessel 1, is shown in Figure 9.

Figure 9. Catch-tank used in the experiments/ Vessel 2
Reprinted with permission from Parr Instrument Company [50]

The features and dimensions of the two vessels, used later in the simulations, are given in table 1.

Table 1: Features of the vessels used in the experiments

Features	Vessel 1	Vessel 2
Volume (L)	1.66	1.11
Wall thickness (m)	0.018	0.0064
Height (m)	0.118	0.112
Material	316L Stainless Steel	
Maximum allowable working pressure (MAWP), barg	150	131

The two vessels are connected by an insulated stainless steel tubes of two different sizes, with 1/8" and 1/16" outer diameter (OD), while keeping the length of the tube constant at 0.43 m. The inner diameter and thickness of the tubes are given in table 2.

Table 2. Tube dimensions used in the experiments

Vendor	Tube outer diameter, inch	Thickness, inch	Internal Diameter, inch
OMEGA Engineering, INC.	1/8	0.028	0.069
	1/16	0.014	0.0345

A ball valve is placed between the vessels on the vent line near vessel 1. Apart from the vessels and the tube, pressure transducers are placed inside each vessel to measure the pressure. These pressure transducers have response time of 1 millisecond according to the vendors and, for the

scope of this work, can be assumed to be instantaneous. Furthermore, the pressure measured in the experiment and reported in this thesis is the absolute pressure unless stated otherwise. The k-type thermocouples are placed inside the vessels to measure the fluid temperature during the depressurization process. The time-constant for these thermocouples is 3 seconds as per vendor's website [51]. The details of pressure transducers and thermocouples used in the experiments is given in Table 3. The overall setup is shown in Figure 10.

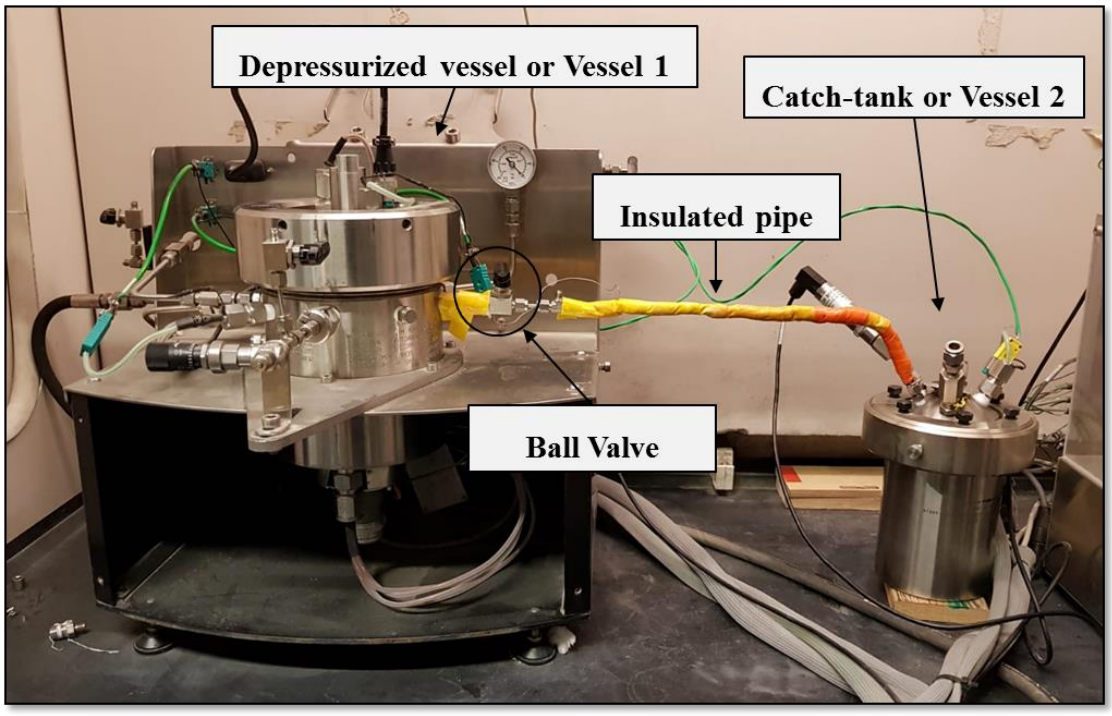

Figure 10. The overall experimental setup

Table 3. Model and uncertainty of the sensors used in the experiments

Sensors	Brand	Model	Sensitivity
Pressure Transducer	OMEGA Engineering, INC.	MMA2.5KV1P1MC673A5CE	±2 psia
Thermocouples (k-type)	OMEGA Engineering, INC.	HFS-4	±1.1°C

Air, nitrogen and helium gas were depressurized from the vessel in the experiments conducted in this work. The selection of these gases were based on the fact that air is a mixture of two diatomic gases, nitrogen is a single diatomic gas and helium is a monoatomic gas with a relatively low heat capacity. The purity and composition of each gas used is given in Table 4.

Table 4. Gas compositions used in the experiments

Vendor	Gas	Purity
National Industrial Gas Plants (NIGP)	Air	79% Nitrogen, 21% Oxygen
	Nitrogen	99.995%
	Helium	99.9995%

4.2.2 Experiment procedure

Nearly all the experiments performed in this work follow the same procedure, except for experiments performed with the mixture of gases, in which extra care was taken to ensure there was no backflow to the gas cylinders. This was done by installing check valves at the inlet of the vessels during the filling process after which the experiment follows the general procedure. The general procedure used for vessel depressurization filled with gas is as follows:

1) Each vessel is flushed with the gas which is depressurized in that particular experimental run to make sure there is no impurities.
2) The initial pressure in vessel 2 is 1 bar in all the experiments. This is achieved by initially set both vessels to 1 bar and then closing the valve between the vessels.
3) Vessel 1 is then filled with the gas at the required pressure for the experiments.
4) The equipment starts recording the data at the rate of 30 data points per second.
5) The valve between the vessels is opened to start the flow of the gas from vessel 1 to vessel 2 resulting in the depressurization of the vessel 1.
6) The data is collected till the pressure and temperature become stable, however the data is trimmed from the point when the valve was opened to the point when the percentage difference between the pressures of the two vessels were 0.1% as given by equation (19).

$$\frac{P_1 - P_2}{\frac{P_1 + P_2}{2}} \times 100 = 0.1\% \tag{19}$$

4.2.3 Application of first order dynamics to the temperature data

A sensor's response to a dynamically changing measurand can be different from an invariable measurand. When dealing with a dynamic system whose measured variable changes rapidly as compared to the intrinsic dynamics of the sensor, such as temperature measurements with the thermocouple, it is necessary to account for the transient properties of the sensing system. These dynamic characteristics exist because of the presence of energy storing elements, which can be electronic, such as inductance or capacitance, mechanical, as for example vibration paths, and related to the mass and thermal elements in the sensor, such as heat capacity [52]. If the output shows the response to the input signal without delay, then the system can be considered as zero-order. However, if the output reaches its final value with a delay, presence of a time-constant or response time, then the system can be represented as first-order.

The dynamic characteristics of the sensors can be observed in the conducted depressurization experiments as the both pressure transducer and thermocouple have a time constant. However, the response time for pressure transducers is very small (1 millisecond) therefore the pressure output can be assumed to be instantaneous. Meanwhile, the thermocouple response time is 3 seconds, which in comparison with the depressurization time in the experiments is large. Hence, it is treated as a first order system, which mathematically can be represented as [52]:

$$\tau \frac{dT_m(t)}{dt} + T_m(t) = T_{inferred}(t) \tag{20}$$

where $T_m(t)$ and $T_{true}(t)$ are measured and the inferred temperature at time t.

The differential part of the equation (20) is approximated by the difference of the values of temperature and time at data point i and the previous data point $i-1$ as shown in equation (21).

$$\frac{dT_{m,i}(t)}{dt} = \frac{T_{m,i} - T_{m,i-1}}{t_{m.i} - t_{m.i-1}} \tag{21}$$

Therefore, using Equations (20) and (21), the inferred temperatures of both vessels are calculated for each of the experiments conducted. Figures 11 and 12 show the inferred and measured temperatures plotted against time for each vessel, for one of the experiments which involved vessel 1 at 10 bar air, depressurized to vessel 2 containing air initially at 1 bar.

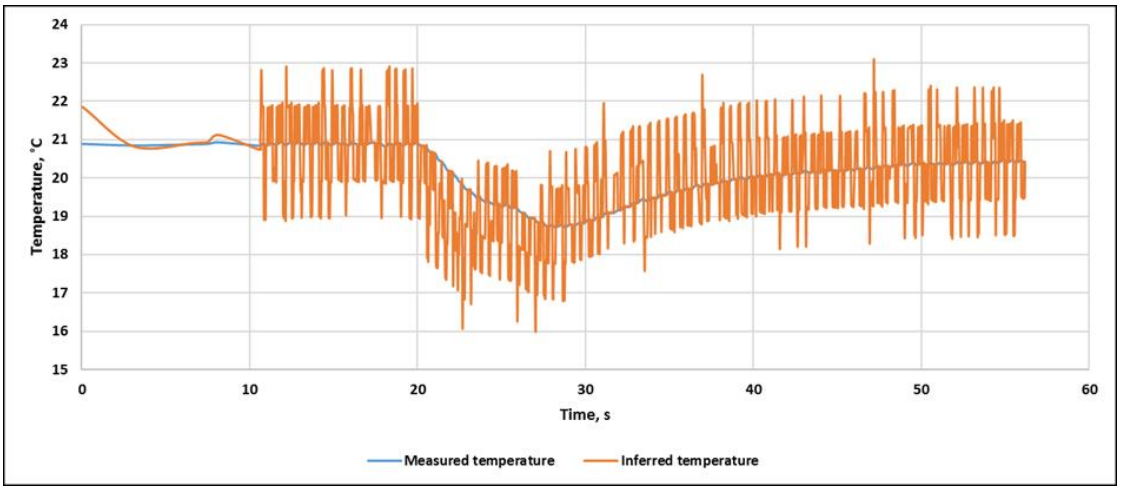

Figure 11. Measured and inferred temperature of vessel 1 after first order dynamics applied

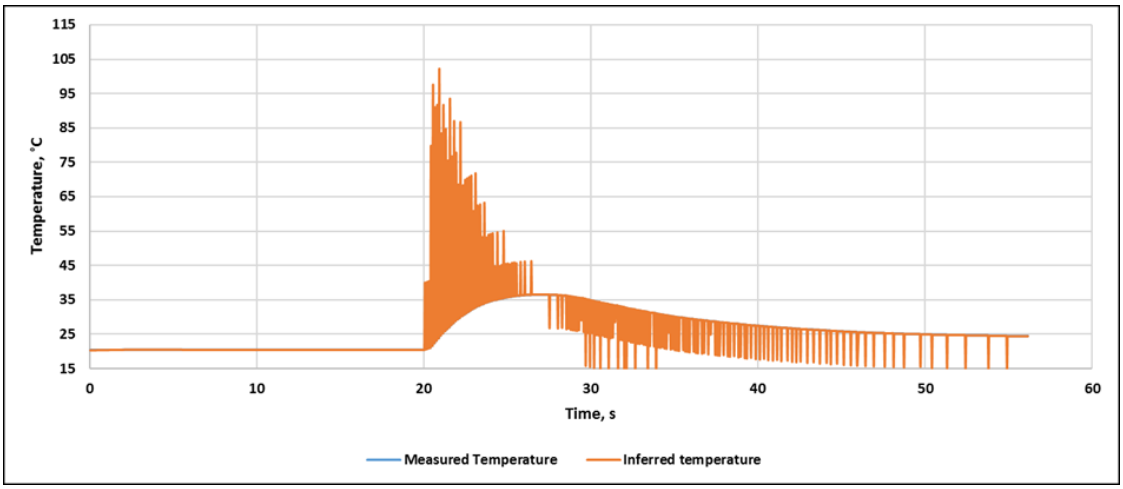

Figure 12. Measured and inferred temperature of vessel 2 after first order dynamics applied

From the plots in Figure 11 and 12, it can be seen that there is a lot of noise in the inferred temperature data due to the derivative present in Equation (20). Therefore, a moving average technique is employed for this term to reduce the noise in the data, which is shown in Equation (22).

$$\left(\frac{dT(t)}{dt}\right)_{average,i} = \frac{\sum_{p=i-1}^{i-\frac{n_{dp}}{2}} \left(\frac{dT(t)}{dt}\right)_p + \left(\frac{dT(t)}{dt}\right)_i + \sum_{q=i+1}^{i+\frac{n_{dp}}{2}} \left(\frac{dT(t)}{dt}\right)_q}{n_{dp}} \tag{22}$$

where i is the number of data point and n_{dp} is the total number of data points used for averaging. It was observed that when a higher value of n_{dp} was used, the noise was reduced significantly. Figures 13 to 16 show the effect of the averaging using n_{dp} at 25 and 75 data points respectively.

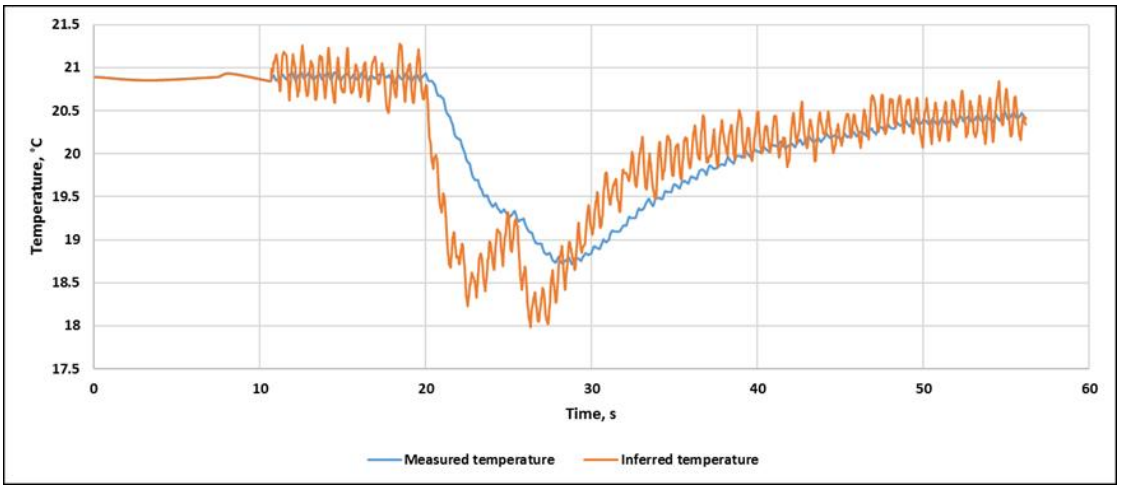

Figure 13. Inferred temperature for vessel 1 after applying moving average technique (25 data points)

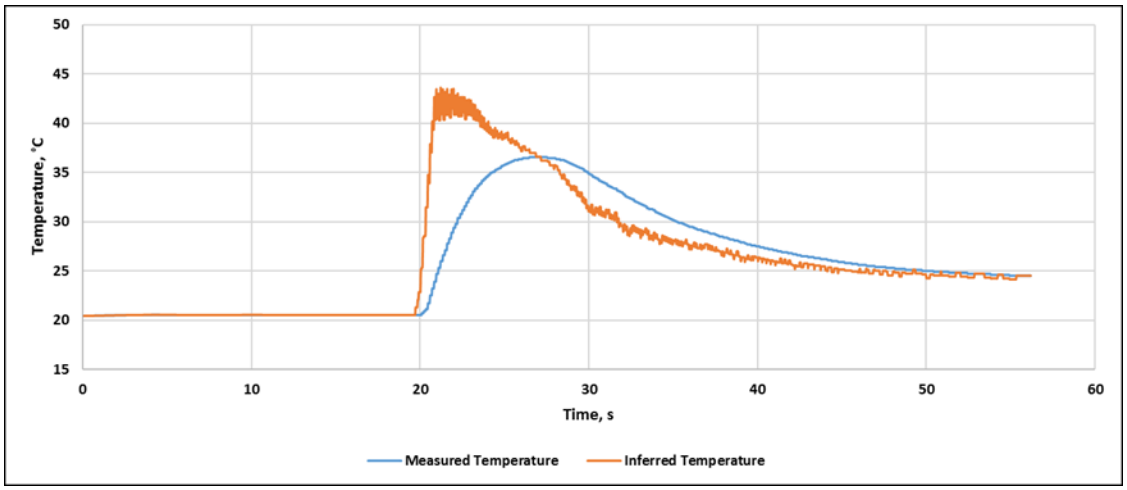

Figure 14. Inferred temperature for vessel 2 after applying moving average technique (25 data points)

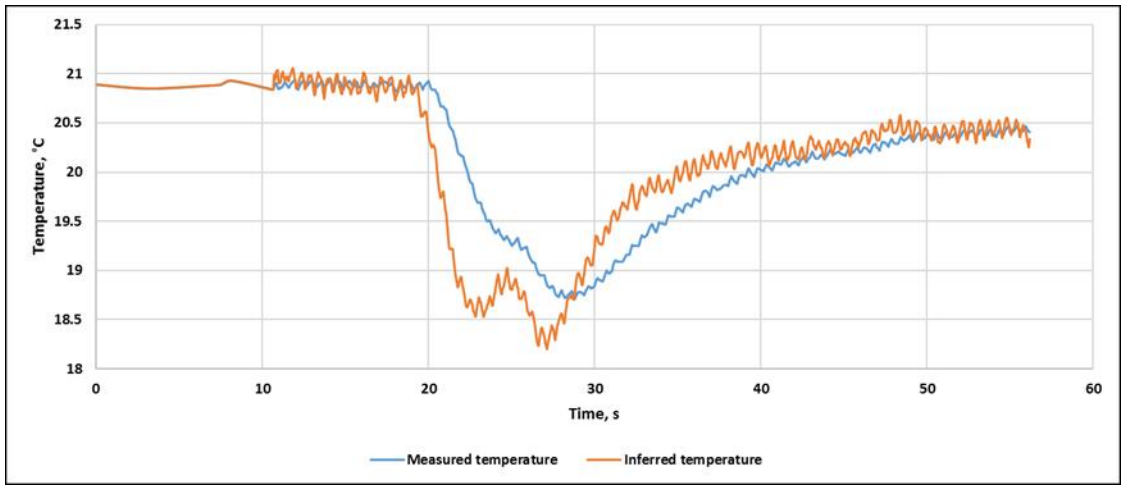

Figure 15. Inferred temperature for vessel 1 after applying moving average technique (75 data points)

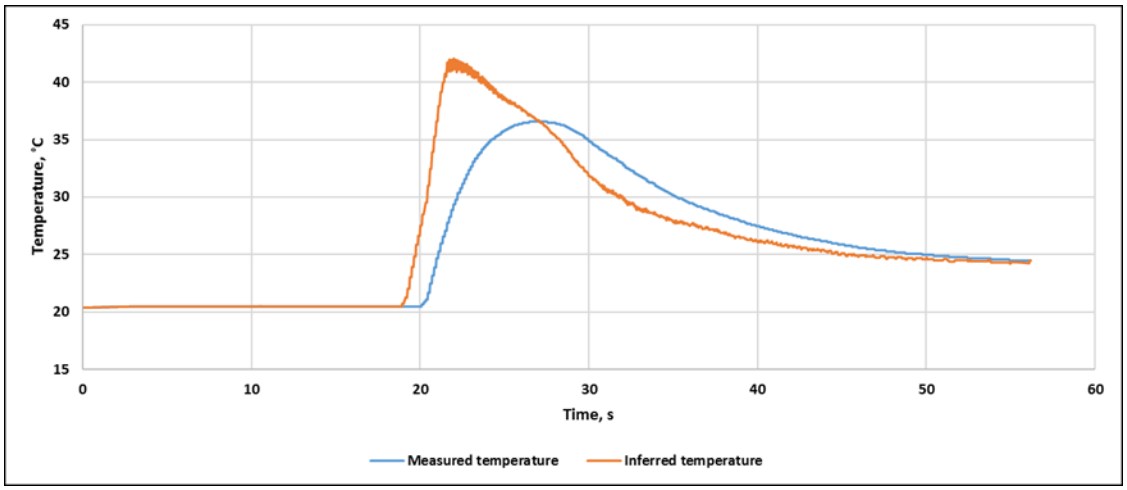

Figure 16. Inferred temperature for vessel 1 after applying moving average technique (75 data points)

A comparison of Figures 13 to 16 shows that, when the data points were increased from 25 to 75, the noise in the data was greatly reduced and an improved result was obtained. Therefore, this technique was applied to all the experimental data.

4.2.4 Calibration process for discharge and heat transfer coefficient

Based on the previously stated methodology, the results from experiments and simulations were compared. It was found that the values of the discharge coefficient and the heat transfer coefficients adopted in the model have large impact on the prediction of accurate depressurization time, and temperature and pressure profiles for each experiment. As an example, the depressurization of an air-filled vessel vented to a catch-tank through a 1/8-inch tube (base case) whose initial conditions are given in the table 5 which is simulated and compared with the experimental results, as shown in Figures 17 and 18 for which the values of discharge coefficient and heat transfer coefficient are given in table 6.

Table 5. Initial conditions of venting through a 1/8-inch tube for the calibration of discharge and heat transfer coefficients

Gas	Tube size	Vessel 1		Vessel 2	
		Pressure (bar)	**Temperature (°C)**	**Pressure (bar)**	**Temperature (°C)**
Air	1/8-inch	10	20.9	1	22.3

Table 6. Discharge coefficients and heat transfer coefficients for initial comparison of experimental and simulation results

Parameters	Typical value	Selected
Discharge Coefficient C_d	0.61 for sharp edged orifice [7]	0.61
h_{conv} (vessel 1), W/m^{2}K	25 to 250 for gases [46]	250
h_{conv} (vessel 2), W/m^{2}K		

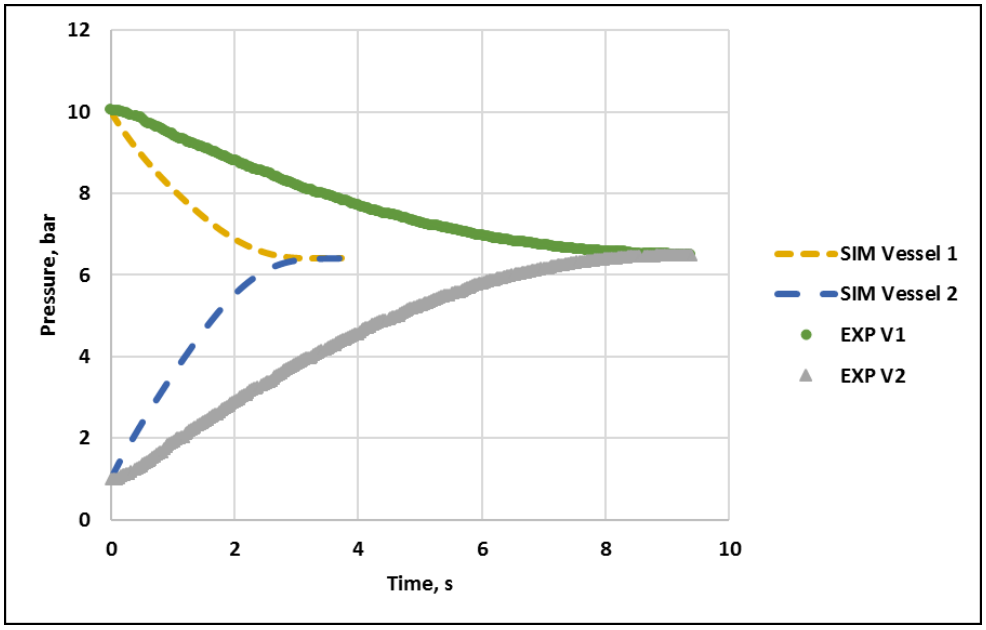

Figure 17. Pressure profile for initial comparison of experimental and simulation results

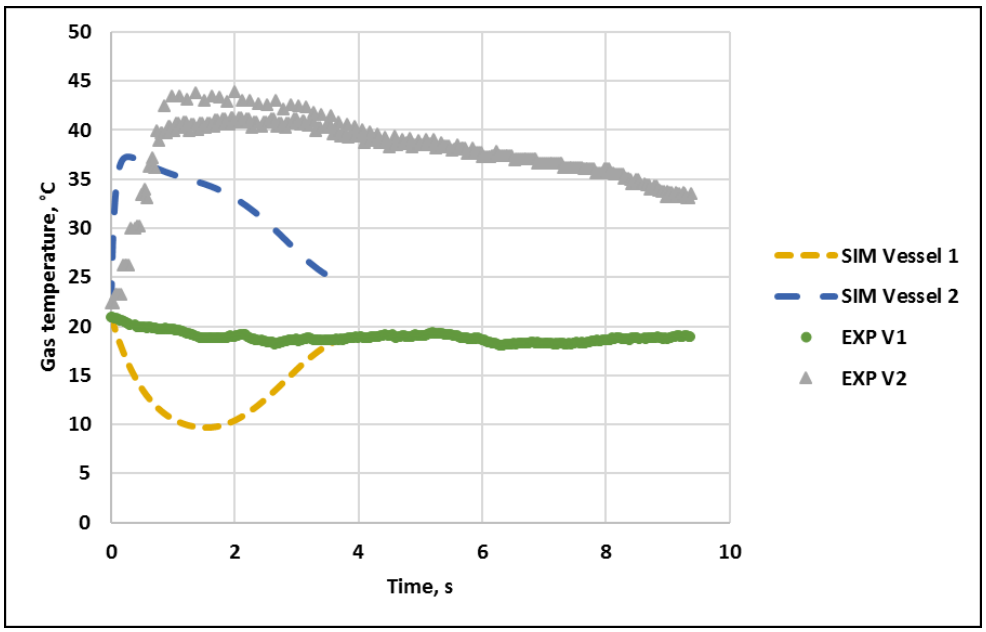

Figure 18. Temperature profile for initial comparison of experimental and simulation results

From Figures 17 and 18, it can be seen that, with the values given in table 3 for discharge coefficient and heat transfer coefficients, the depressurization time is greatly under predicted. In addition, although the model is able to predict the equilibrium pressure, there are disagreements in the temperature profiles between experimental and simulation data that cannot be ignored. Therefore, to rectify this issue, the values of discharge coefficient and the heat transfer coefficient are calibrated for a base case (experiment) whose details are given in table 3 by carrying out multiple simulations through manipulation of the values of the coefficients to match the depressurization time and the maximum temperature predicted by the simulation to the experiments. This process is shown in table 7 where V1 and V2 stands for vessel 1 and vessel 2 respectively.

Table 7. Calibration of discharge and heat transfer coefficient for 1/8-inch tube

Original Diameter (m)	Cd	Reduced Diameter (m)	Heat transfer Coefficient (W/m2.K)		Experiments			Simulation		
			V1	V2	Temp V1 (°C)	Temp V2 (°C)	EXP time (s)	Temp V1 (°C)	Temp V2 (°C)	SIM time (s)
1.75E-03	0.36	1.05E-03	20	20	18.21	42.08	9.38	-0.47	68.58	9.81
1.75E-03	0.36	1.05E-03	80	80	18.21	42.08	9.38	4.41	45.50	7.00
1.75E-03	0.36	1.05E-03	200	80	18.21	42.08	9.38	11.98	45.48	6.32
1.75E-03	0.25	8.76E-04	400	180	18.21	42.08	9.38	17.80	31.16	7.84
1.75E-03	0.24	8.59E-04	350	60	18.21	42.08	9.38	16.99	44.37	11.39
1.75E-03	0.3	9.60E-04	350	60	18.21	42.08	9.38	16.12	47.99	10.40
1.75E-03	0.36	1.05E-03	350	60	18.21	42.08	9.38	15.32	51.13	7.70
1.75E-03	0.36	1.05E-03	400	100	18.21	42.08	9.38	15.90	42.61	6.15
1.75E-03	0.3	9.60E-04	400	100	18.21	42.08	9.38	16.67	40.07	7.42
1.75E-03	0.3	9.60E-04	375	80	18.21	42.08	9.38	16.40	43.28	7.53
1.75E-03	0.25	8.76E-04	375	80	18.21	42.08	9.38	17.40	40.66	8.51
1.75E-03	0.25	8.76E-04	375	60	18.21	42.08	9.38	17.09	45.05	12.97
1.75E-03	0.25	8.76E-04	375	70	18.21	42.08	9.38	17.06	42.62	8.59
1.75E-03	**0.25**	**8.76E-04**	**375**	**65**	**18.21**	**42.08**	**9.38**	**17.06**	**43.77**	**9.45**
1.75E-03	0.27	9.11E-04	375	65	18.21	42.08	9.38	17.03	44.96	10.35
1.75E-03	0.27	9.11E-04	375	70	18.21	42.08	9.38	16.79	43.74	8.14
1.75E-03	0.24	8.59E-04	375	70	18.21	42.08	9.38	17.20	43.15	10.49

From this method, values for the discharge coefficient and heat transfer coefficient were obtained. However, when the tube diameter is changed from 1/8-inch to 1/16-inch, the calibration is required again because the diameter of the orifice is now changed and the discharge coefficient will alter as well. Therefore, a similar process as shown in table 7 is repeated for the 1/16-inch tube but, this time, only the discharge coefficient is manipulated to match the depressurization time while keeping the heat transfer coefficients the same as those for the 1/8-inch tube. Table 8 provides the details of the initial conditions for the experiment used to calibrate the discharge and heat transfer coefficients for venting of a gas through 1/16-inch tube.

Table 8. Initial conditions of venting through a 1/16-inch tube for the calibration of discharge and heat transfer coefficients

Gas	Tube size	Vessel 1		Vessel 2	
		Pressure (bar)	Temperature (°C)	Pressure (bar)	Temperature (°C)
Air	1/16-inch	10	21.9	1	23.5

The values of the coefficients found using this process, given in Table 9, are used for the simulation of all the experiments.

Table 9. Summary of calibrated discharge and heat transfer coefficients

Parameters	Calibrated Values	
	1/8-inch	1/16-inch
Discharge Coefficient C_d	0.25	0.18
h_{conv} (vessel 1), W/m^2K	375	375
h_{conv} (vessel 2), W/m^2K	65	65

The extremely low values of discharge coefficient obtained using calibration process as shown in Table 9, indicates that the fluid may encounter another discharge coefficient at the entrance of the vessel 2 along with the discharge coefficient at the exit of vessel 1. A combined effect from both of these coefficient at the entrance and exit may have caused a lower value for the discharge coefficient found using the calibration.

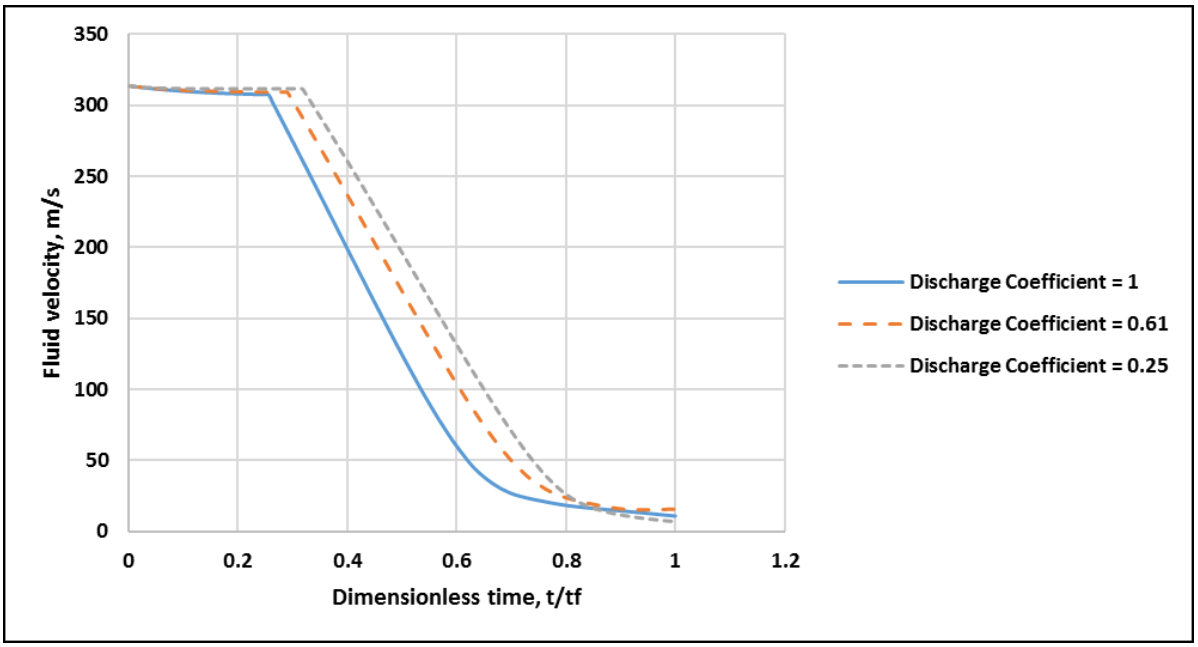

Figure 19. Fluid velocity as a function of dimensionless time at different discharge coefficient

Figure 19 shows fluid velocity as a function of dimensionless time. The simulation was run for the conditions given in Table 5 using different values of discharge coefficient. Overall, it can be seen that the initial velocities and final velocities for any value of the discharge coefficient is the same. The fluid is at the constant sonic speed in the beginning of the simulation because of the choked flow condition and just as the fluid flow becomes non-choked, the velocity starts decreasing. It can also be seen that the discharge coefficient does not significantly affect the velocity of the fluid and on average the gas spends a little time in the tube before filling into the other vessel as shown in the table below shows the average speed and time taken by the gas to flow through the tube connecting each vessels.

Table 10. Average speed and average time spent in the tube at different discharge coefficient

Discharge Coefficient	1	0.61	0.25
Average speed, m/s	239.4	250.4	259.0
Length of the tube, m	0.43		
Average time, s	0.00180	0.00172	0.00166

4.2.5 Experimental campaign

In this work, the depressurization of a vessel containing non-reacting gases vented to a catch-tank is studied via experimentations and simulation of the process. Multiple experiments have been conducted by varying different factors which would impact the depressurization process. The data generated is then also used to validate the results from the extended simulator and to observe if the simulator can predict the impact of the variation as well. This process not only helps to identify the weak points in the simulator but also helps to develop a deeper understanding of the dynamic phenomena that take place during depressurization.

Table 11 shows the experimental plan developed to study the variation of factors that would impact depressurization.

Table 11. Experiments performed for validation and study of different factors affecting depressurization

Varying Factors	Description
Initial pressure in vessel 1	• Air depressurized from vessel 1 at variety of initial pressures ranging from 3-50 bar • Vessel 2 always at 1 bar containing air
Nature of gas	• Air, nitrogen or helium depressurized from vessel 1 initially at 25 bar pressure • Vessel 2 at 1 bar containing the same gas as vessel 1
Composition in mixture of gases	• Vessel 1 containing mixture of air, nitrogen and helium varying the composition o Equimolar o 53.3% N_2, 33.3% Air, 13.3% He o 13.3% N_2, 33.3% Air, 53.3% He • Vessel 2 contains air at 1 bar pressure for all the experiments
Tube diameter	• Vessel 1 depressurized containing air at 25 bars conducted on two different tube diameters: o 1/8 inches OD o 1/16 inches OD • Vessel 2 contains air at 1 bar for each case

5. RESULTS

The results of the experiments and simulation will be presented in this section which would include for each case, a plot for pressure and temperature in each vessel. The thermodynamic properties of the components that were simulated such as critical temperature, critical pressure, acentric factor and heat capacity as a function of temperature have been obtained using Knovel DIPPR Project 108 [53]. In the simulations that follow, each vessel is assumed to be made of stainless steel 316L for which the heat capacity is given as the function of temperature [54] as shown in equation (23).

$$C_{p,steel}(\frac{J}{kg.K}) = 357.36 + 0.20011T - 2.00010 \times 10^{-7}T \quad (23)$$

The thermal conductivity is assumed to be constant and has been reported to be 16.3 W/m.K [55].

5.1 Simulation Results

After the dynamic simulator was extended to simulate multiple vessels, a depressurization of a vessel filled with air (79% Nitrogen, 21% Oxygen), which was vented to a catch-tank through a 0.05 meters of orifice diameter, was simulated. The mass of the vessel was assumed to be very small to neglect the effect of heat transfer. This section also shows the kind of results the extended simulator is capable of generating. Figure 20 shows the schematic of the simulated process. Table 12 shows the key parameters used in the simulation.

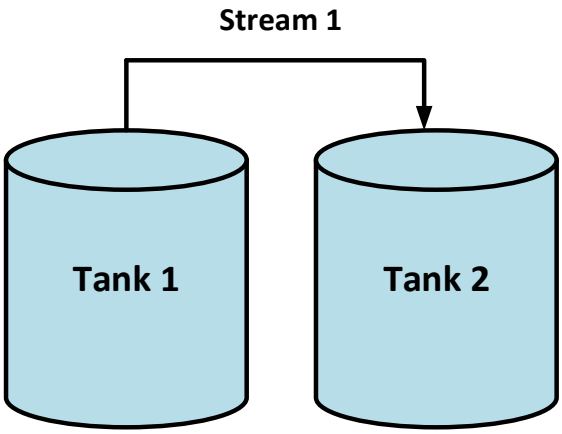

Figure 20. Process Schematic

Table 12. Initial conditions for simulation of air depressurized from tank 1 to tank 2

	Tank 1	**Tank 2**
Temperature, °C	226.85 (500 K)	226.85 (500 K)
Pressure, bar	1.5	1
Amount of N_2, mol	3.135	2.09
Amount of O_2, mol	0.8325	0.555
Volume, L	110	110

The pressure, temperature and number of moles profile is generated by the simulator during the depressurization of a vessel at 1.5 bar to a vessel at 1 bar. The results are shown in Figure 21.

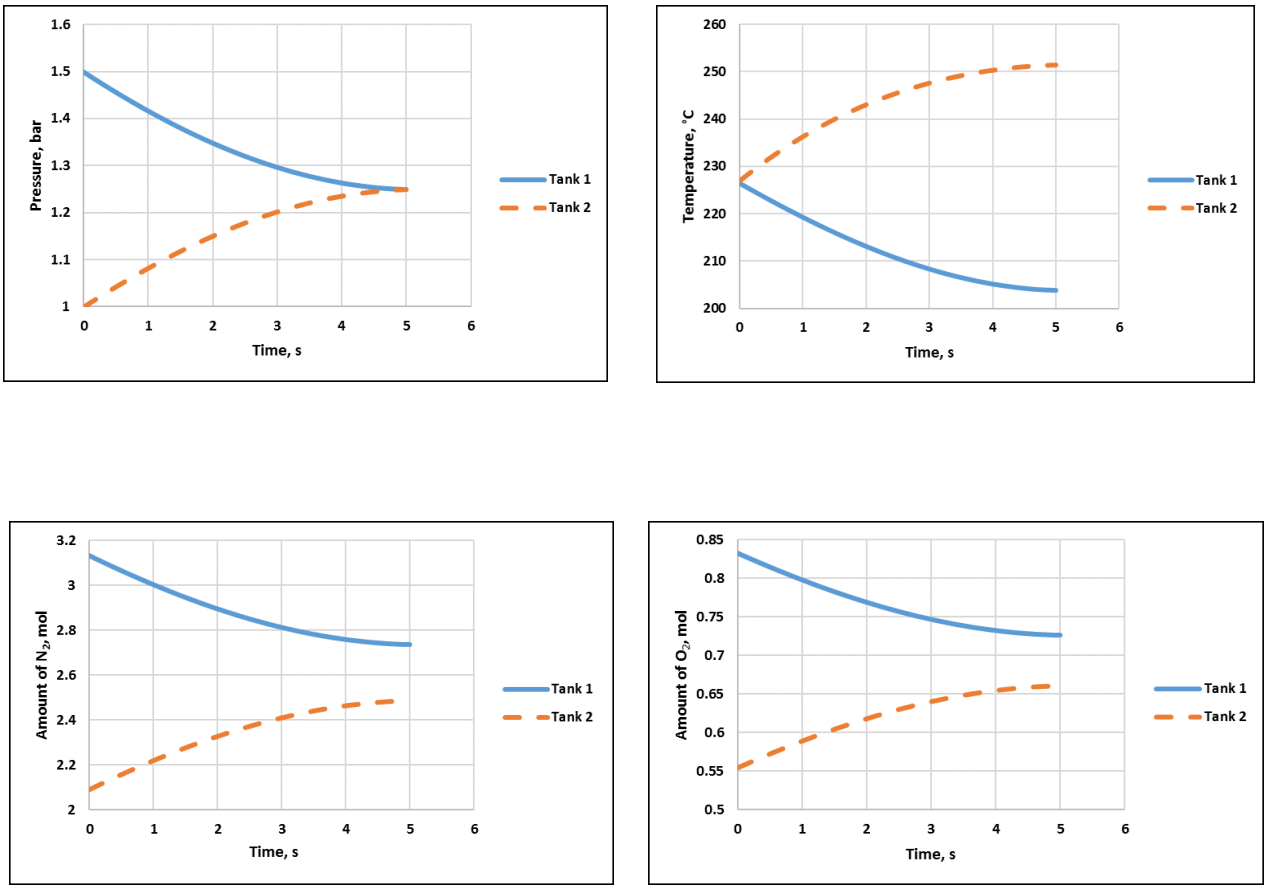

Figure 21. Results from the simulator showing temperature, pressure and component amounts as a function of time in each tank

The symmetric profiles in the simulator can be seen because the vessel have exact same mass and volume. The pressures are expected to fall in the depressurizing vessel (tank 1) and simultaneously cause increase in the tank 2 which can be seen in the graphs obtained from the simulation. The internal energy is carried by the mass leaving tank 1 and being added to the catch tank which results in the decrease and increase in tank 1 and tank 2 respectively. The symmetry in the temperature profile is because same energy that leaves tank 1 is added to tank 2. For the amount of nitrogen and oxygen in tanks, an expected decrease in the number of moles can be observed in

tank 1 while the amount increases in tank 2 during the process. However, there is no equilibrium between the mass of the fluid in vessel as the mass transfer is not considered in the simulator. The results obtained for the process shows expected trends, therefore confirming the capability of handling multiple vessels by the extended dynamic simulator.

5.2 Validation of the results with EMSO

The results from the extended dynamic simulator were validated against simulations conducted on EMSO using same initial conditions and vessel dimensions. The validation is shown in Figures 22-24. However, it is to be noted that, due to the lack of a sound speed calculation algorithm in EMSO, the molar flowrate of the exit stream was given by a simple equation for the sake of comparison. Nonetheless, it is interesting to compare the relationship between the amount of the component in the tank and the corresponding temperature and pressure. Therefore, the comparison between the two simulators was not made on time scale but rather by two methods:

1) Temperature as a function of pressure in the vessel shown in Figure 22;
2) Temperature and pressure as a function of the amount of nitrogen in vessel 2, shown in Figures 23 and 24.

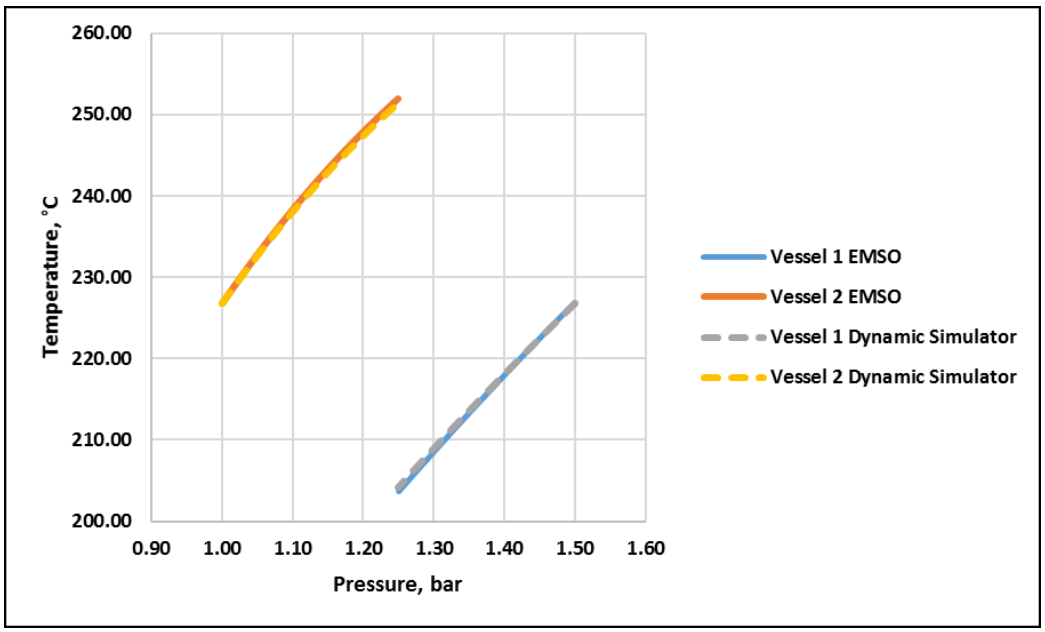

Figure 22. Validation of the extended simulator with EMSO: temperature as a function of pressure in each vessel

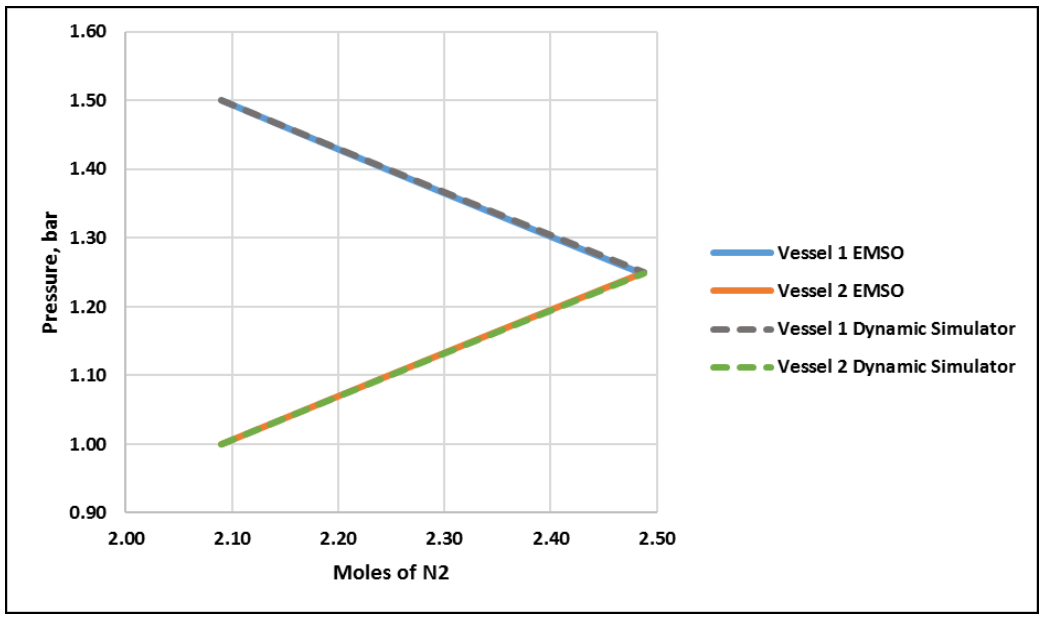

Figure 23. Validation of the extended simulator with EMSO: pressure as a function of the amount of nitrogen in vessel 2

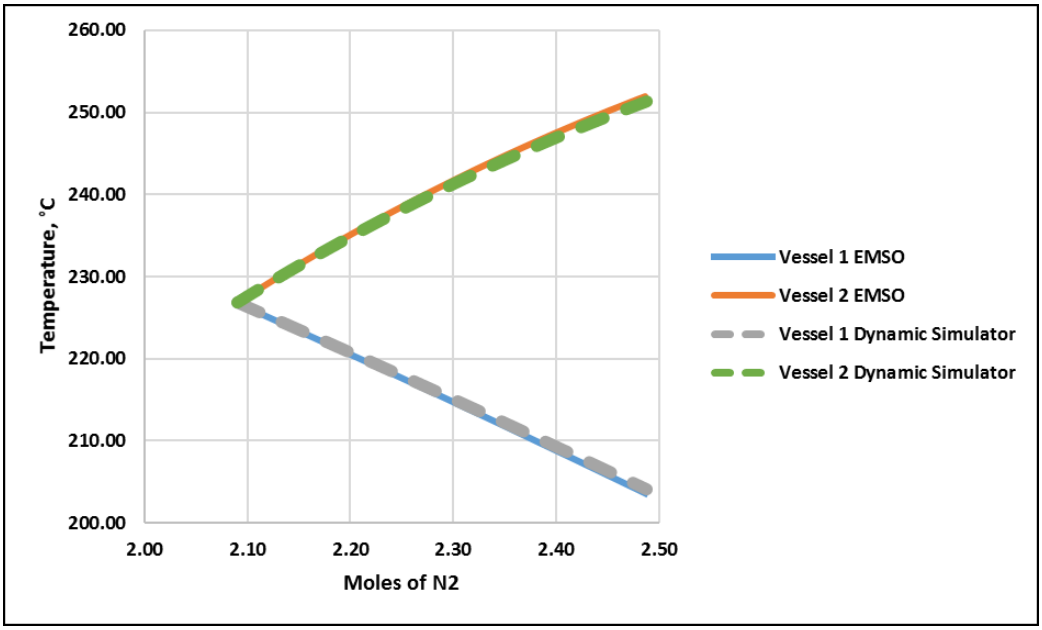

Figure 24. Validation of the extended simulator with EMSO: temperature as a function of the amount of nitrogen in vessel 2

The results of EMSO and of the extended simulator for the temperature and pressure profiles, plotted in this way, are in excellent agreement.

5.3 Wall temperatures from the simulation

After the results were validated with EMSO, the heat transfer differential equations were added to the simulator. Since, there are different nodes assumed to be between the inner and outer wall of the vessel, a temperature gradient in the wall can be observed through simulation results, which shows the potential of the simulator to predict the dynamic changes in the vessel wall.

For a case where air was depressurized from vessel 1 at 49.83 bar and 24.03°C and vented to vessel 2 also containing air, which is initially at 1.00 bar and 36.52°C through a 1/8-inch tube, the simulation predicts the temperature profile of 8 nodes between inner and outer walls of each vessel, as shown in Figures 25 and 26.

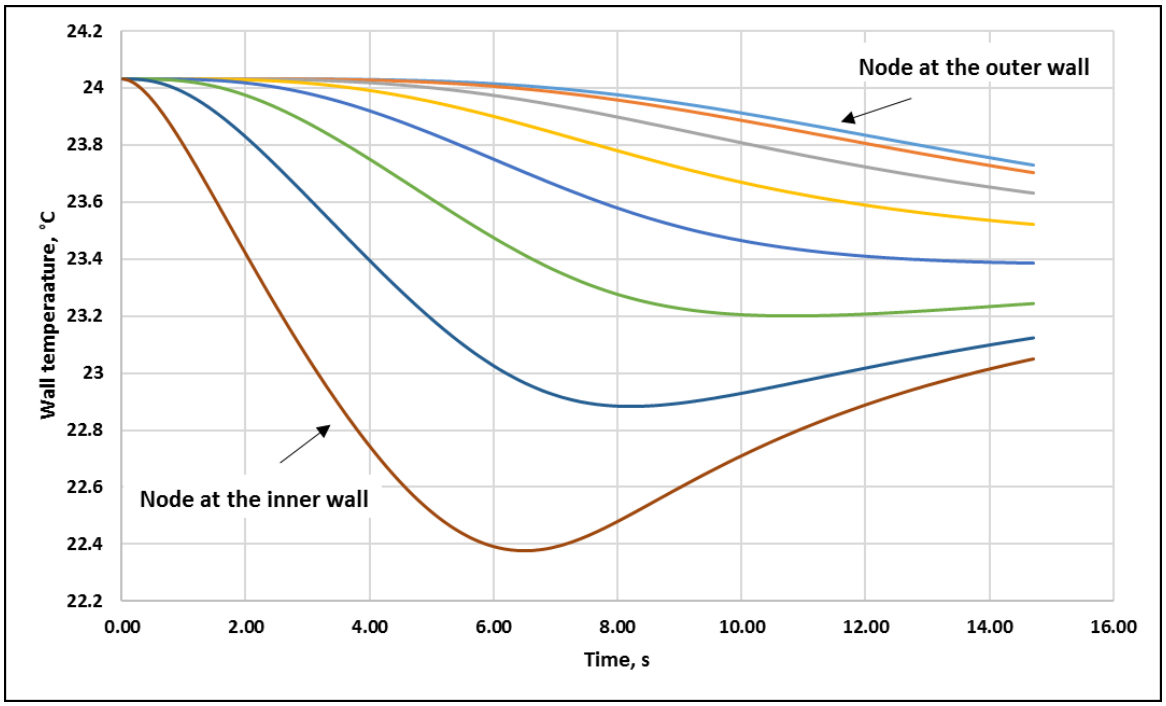

Figure 25. Wall temperatures at each node in vessel 1 predicted by the simulator

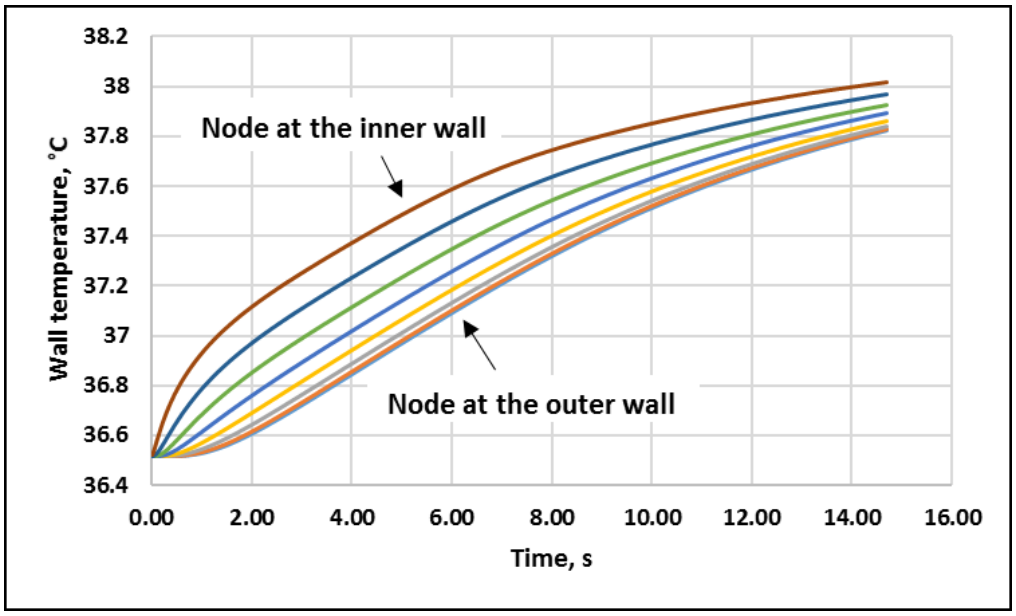

Figure 26. Wall temperatures at each node in vessel 2 predicted by the simulator

The node at the inner wall shows significant change in each vessel because the node is exchanging heat with the fluid in the vessel which causes the temperature change throughout the thickness of the vessel wall as the outer wall is assumed to be insulated. Another interesting observation is that in vessel 1 the temperature drops quickly due to the depressurization but then starts rising as the temperature gradient in the vessel wall becomes significant and leads to heat transfer through conduction in the vessel wall.

5.4 Mass sensitivity on fluid temperature in the vessel

The mass of the vessel was varied up to ± 50% of its original mass by manipulating the thickness of the vessel used given in Table 1. The experiment conditions given in the Table 5 were simulated using different values of the mass of the vessel being depressurized.

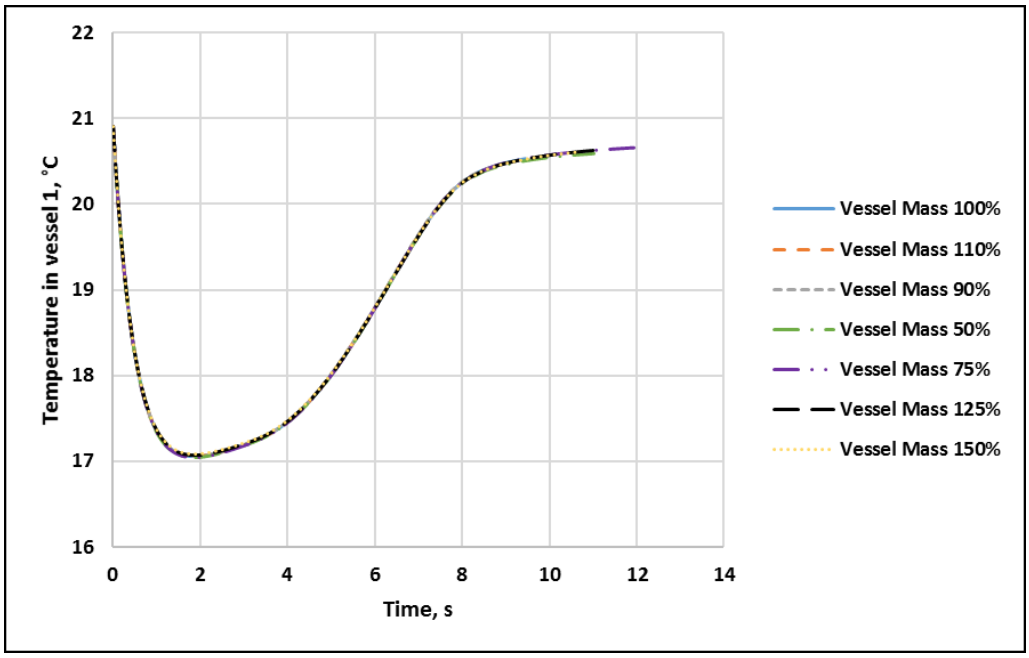

Figure 27. Mass sensitivity on fluid temperature

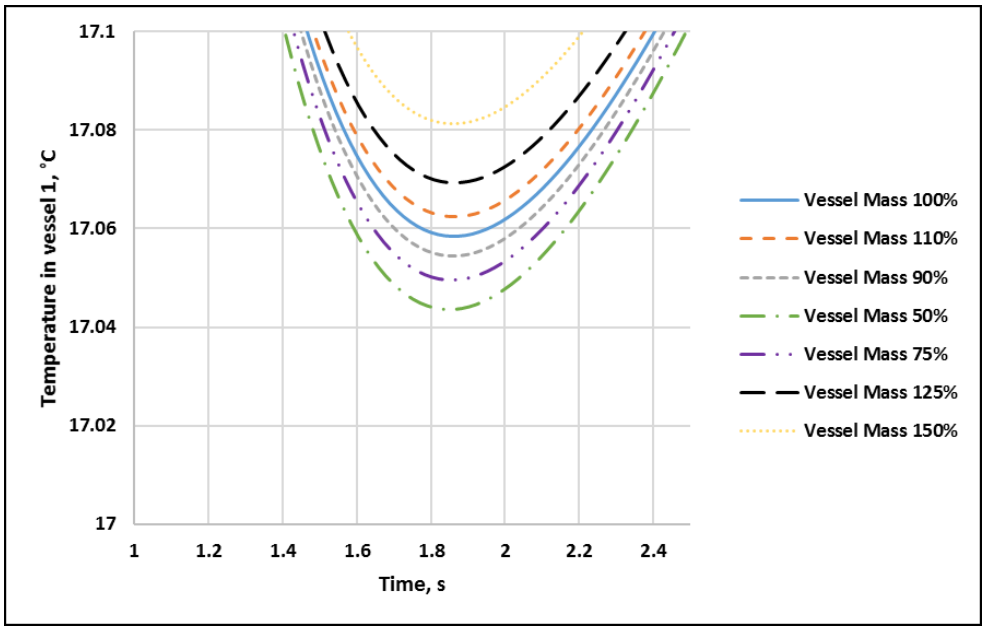

Figure 28. Mass sensitivity on fluid temperature (zoomed in)

The results are plotted in the figure 27, which shows that temperature of the gas in the vessel is not sensitive to the mass or thickness of the vessel used in the calculation. Therefore, uncertainty associated with the measurement and calculation of the vessel mass does not significantly produce a change in the obtained results. However, it is expected that as the mass of the vessel increases, heat transfer to walls of the vessel may increase causing a lower drop of temperature in the depressurizing vessel. Though the change is insignificant, when zoomed in the plot (figure 27) at the point of lowest drop in temperature shown in figure 28, it can be seen that expected behavior is observed. Similarly, the drop in temperature of the depressurizing vessel is high when a relatively lower vessel mass is used in the simulation due to less effect from the heat transfer to the walls of the vessel.

5.5 Impact of varying initial pressures on the depressurization

Air (79% N_2, 21% O_2) at different initial pressures in vessel 1 is depressurized and vented to a catch-tank called vessel 2, through a 1/8-in tube, filled with air at 1 bar. Table 13 shows the experimental conditions for each graph presented in this section.

Table 13. Initial conditions to study the effect of different initial pressures

No.	Vessel 1		Vessel 2	
	Pressure (bar)	Temperature (°C)	Pressure (bar)	Temperature (°C)
1	49.83	24.03	1.00	36.52
2	25.06	22.12	1.00	32.35
3	10.05	20.91	1.00	22.34
4	5.03	20.87	1.01	20.84

The experimental and simulation results for both vessels are given in Figures 29 and 30, showing the pressure and temperature profiles during the depressurization process.

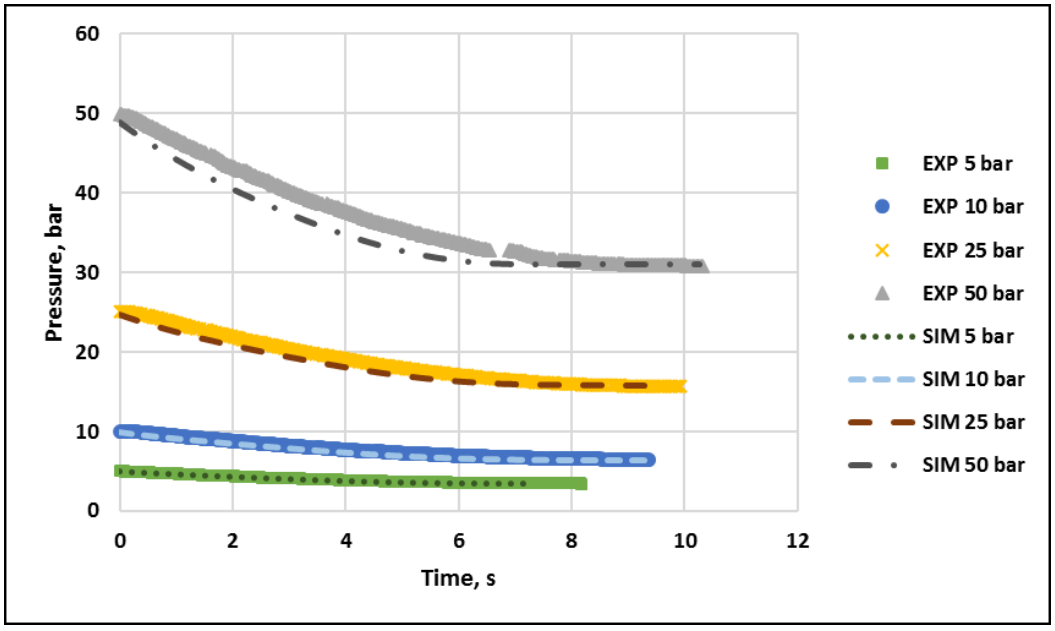

Figure 29. Pressure profiles in vessel 1 for depressurization at different initial pressures

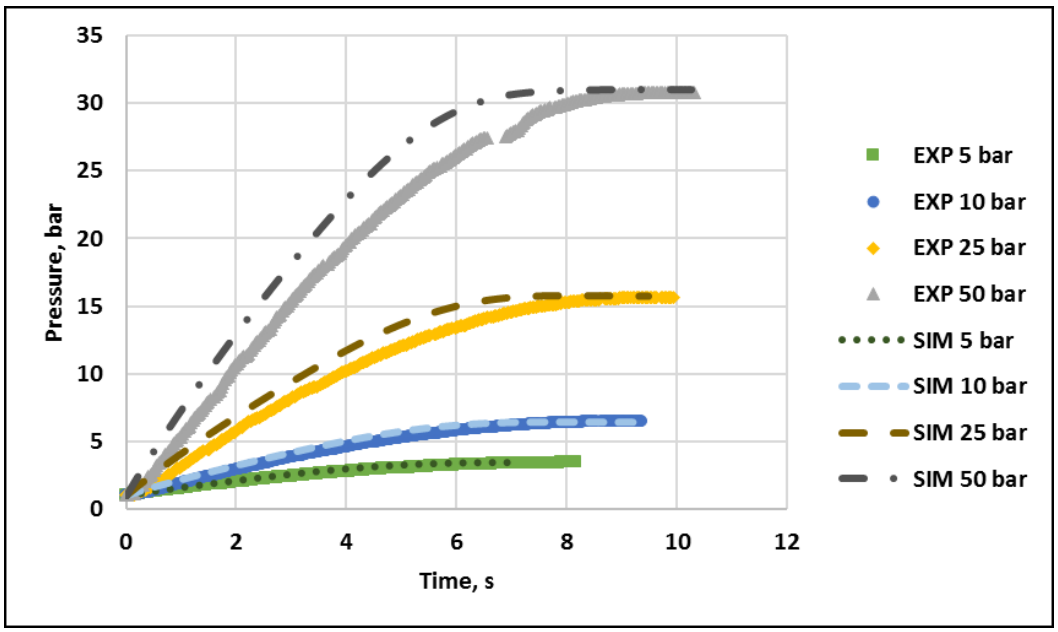

Figure 30. Pressure profiles in vessel 2 for depressurization at different initial pressures

It can be seen from Figures 29 and 30 that, as the initial pressure increases, the depressurization time also increases. The slope of the pressure profiles is steep in the beginning of each experiment and simulation and plateaus as it comes closer to the equilibrium pressure. This is because the driving force for the flow is the pressure difference between the vessels. Simulation results show good agreement with experimental data for pressure profiles in each vessel. Nonetheless, for the experiment conducted at the initial pressure of 5 bar in vessel 1, it can be seen that the simulator under-predicts the depressurization time; however, the equilibrium pressure is predicted accurately for all the cases.

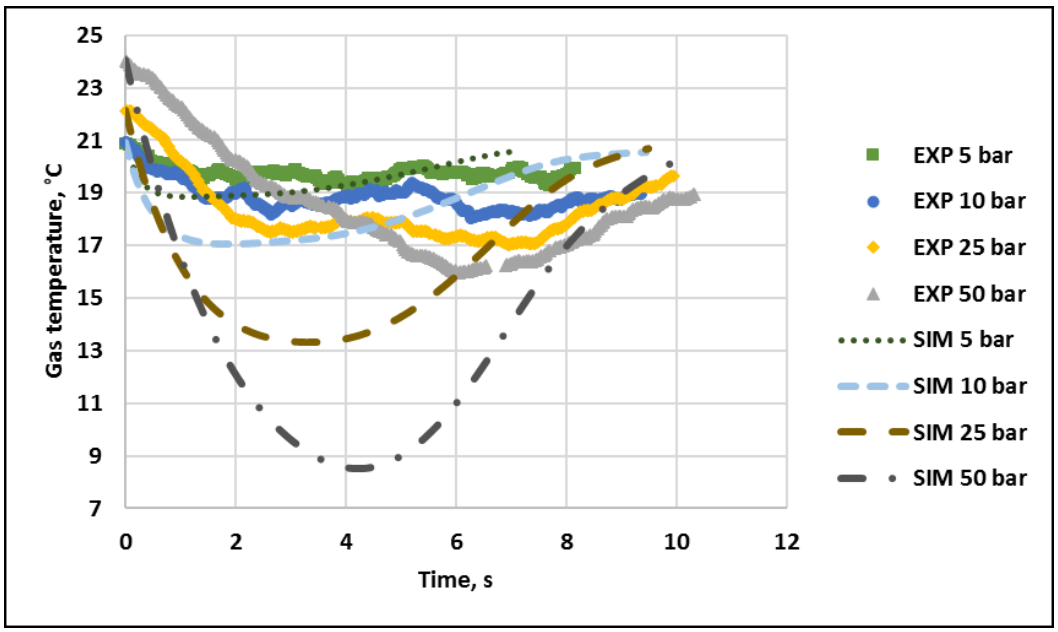

Figure 31. Temperature profiles in vessel 1 for depressurization at different initial pressures

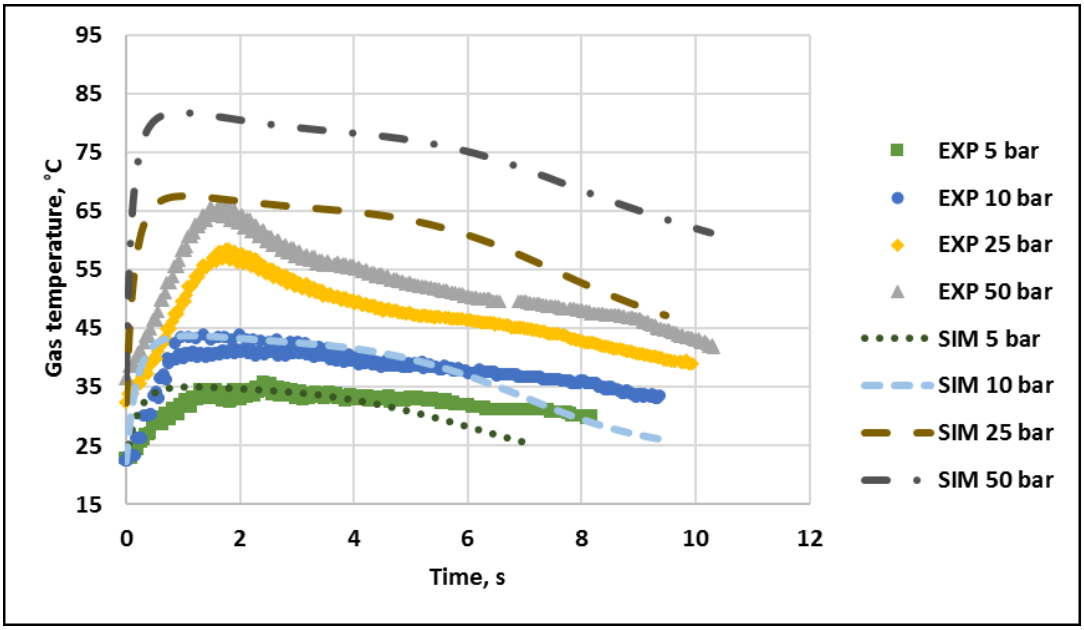

Figure 32. Temperature profiles in vessel 2 for depressurization at different initial pressures

The temperature profiles are presented in Figures 31 and 32, which show that the temperature change in each vessel depends on the initial pressure. So, in general, the higher is the initial pressure in vessel 1, more will be the drop in temperature in vessel 1 and more will be the rise in temperature in vessel 2. The temperature data obtained from the experiments and simulations show that the profiles are unsymmetrical and the drop in temperature in vessel 1 is much lower than the increase in vessel 2. This means that the heat transfer plays a vital role in the determination of the temperature in each vessel. Furthermore, the magnitude of temperature change is also related to the amount of fluid present in each vessel. As seen in the experiments, vessel 2 has relatively less initial mass as compared to vessel 1. Therefore, the inflow of energy in vessel 2 causes a jump in temperature in the beginning of the process. However, this effect is less pronounced in vessel 1 because the same energy change is being absorbed by a larger amount of fluid initially present in vessel 1. Furthermore, at the end of the depressurization process, the temperature seems to come back to the initial temperature due to the heat transfer to the vessel walls becoming dominant. This is because the mass of the vessel is much larger than the gas inside the system therefore contributing to lower change in temperature of the vessel walls than the gas. Consequently, a temperature gradient develops between the gas-wall interface leading to a heat transfer which causes the temperature of the gas to drop and rise for vessel 1 and 2 respectively.

The simulator captures the trend of the experimental results and shows good agreement with them especially for low initial pressures, since the calibration for discharge and heat transfer coefficient was done for 10 bar initial pressure. However, it greatly exaggerates the temperature change for cases with high initial pressures in vessel 1. The likely explanation is that higher pressures in the

vessel result in higher rate of heat transfer to the vessel walls due to higher number of moles present and retention time in the vessel.

5.6 Impact of the nature of gas on the depressurization

Vessel 1 containing different non-reacting gases such as air, nitrogen and helium at 25 bar pressure is depressurized and vented through a 1/8-inch tube to another vessel containing the same gas at 1 bar pressure. The initial conditions are shown in Table 14.

Table 14. Initial conditions to study the effect of nature of the gas

Gas	Vessel 1		Vessel 2	
	Pressure (bar)	**Temperature (°C)**	**Pressure (bar)**	**Temperature (°C)**
Air	25.06	22.12	1.00	32.35
Nitrogen	24.88	20.96	1.00	28.01
Helium	25.08	20.89	1.00	40.95

The comparison is made between the pressure and temperature plots obtained from the experiments and simulation for each vessel. The selection criteria of the gases used in the experiment is the fact that air is a mixture of two diatomic gases while nitrogen and helium are single diatomic and monoatomic gases, respectively.

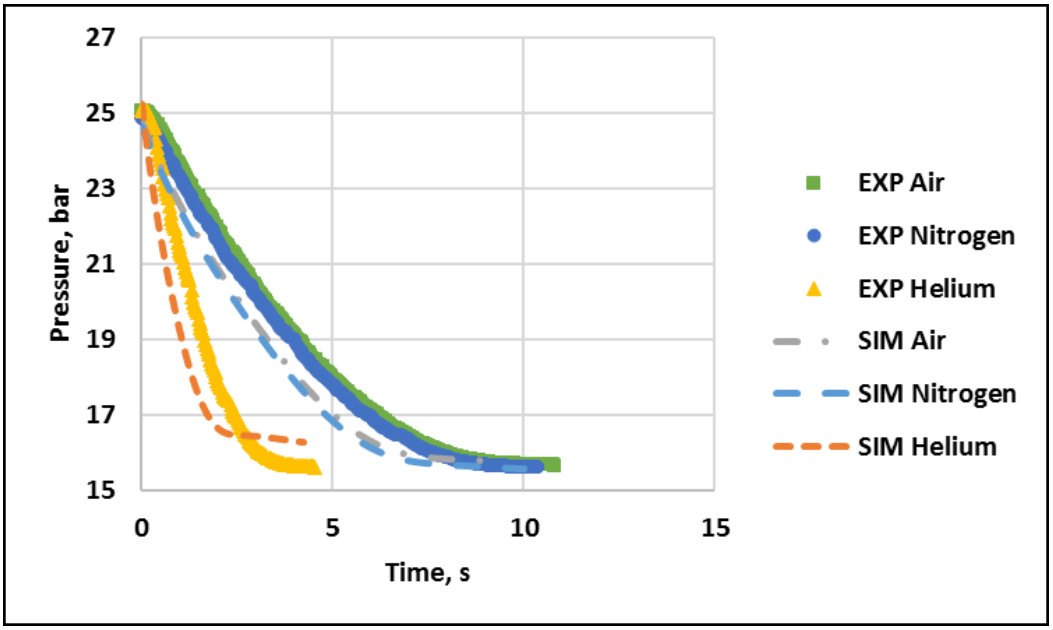

Figure 33. Pressure profiles in vessel 1 for the comparison of the behavior of different gases during depressurization

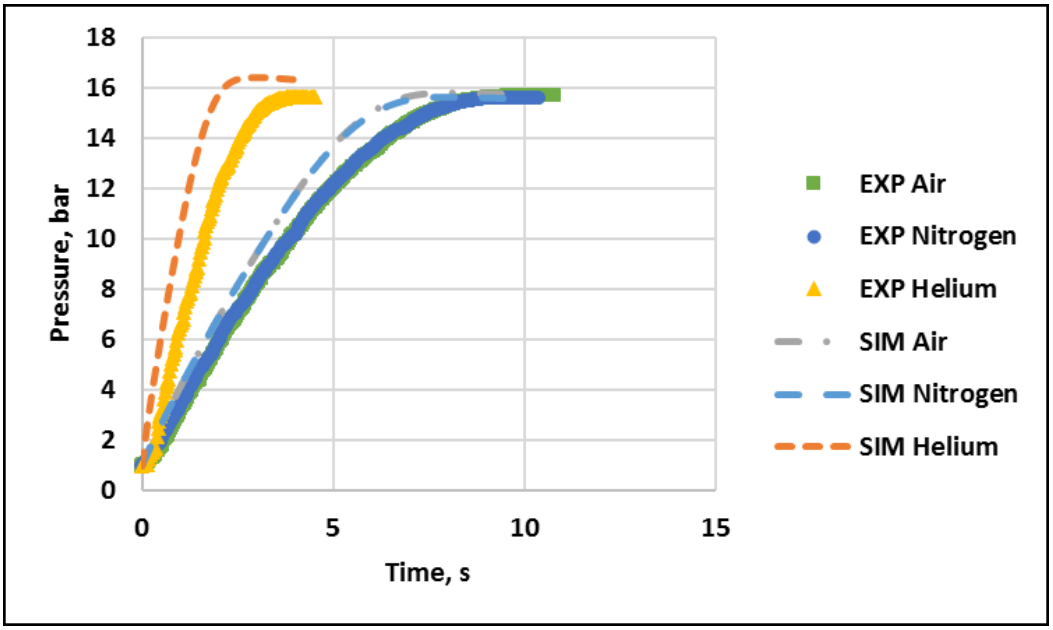

Figure 34. Pressure profiles in vessel 2 for the comparison of the behavior of different gases during depressurization

Figures 33 and 34 show the symmetrical pressure profiles obtained for depressurization experiments and simulation of different gases in each vessel. Since air and nitrogen are similar gases, it can be observed in these figures that the pressure profiles for each gas are very similar. The depressurization time for helium is smaller than for the other two gases because helium has much smaller molar mass than the other gases. The speed of sound in ideal gases is given by Equation (24) below:

$$c_{ideal} = \sqrt{\frac{\gamma RT}{M}} \tag{24}$$

where R is the gas constant, T is the temperature of the gas, γ and M are the heat capacity ratio and molar mass of the gas.

$$\frac{c_{ideal,helium}}{c_{ideal,air}} = \sqrt{\frac{\gamma_{helium} M_{air}}{M_{helium} \gamma_{air}}} \tag{25}$$

Table 15. Molar mass and heat capacity ratio for speed of sound calculation

Gas	Molar Mass (kg/mol) [56]	Heat capacity ratio [56]
Helium	4.0	1.667
Air	28.97	1.4

At the same temperature, the ratio of speed of sound in helium and air, given by Equation (25) calculated using properties listed in table 15, shows that the speed of sound in helium is 2.94 times more than the speed in air. Therefore, at choked flow conditions the depressurization of helium

should be approximately 2.9 times than the air. However, since the backpressure is continuously changing, it is expected that the flow will not be choked at all times therefore from experiments it is found that the depressurization time for helium is 2.3 times more than the air.

In general, there is a good agreement of simulation pressure data with experimental data. However, a slight disagreement can be seen in the pressure behavior of the helium gas because it has been established that the depressurization time, pressure and temperature profiles are sensitive to the discharge and the heat transfer coefficients. The fact that these coefficients were calibrated for air rather than helium possibly explains the mismatch between the experimental and simulation profiles for helium.

The simulator shows good potential for predicting equilibrium pressures for depressurization involving different gases.

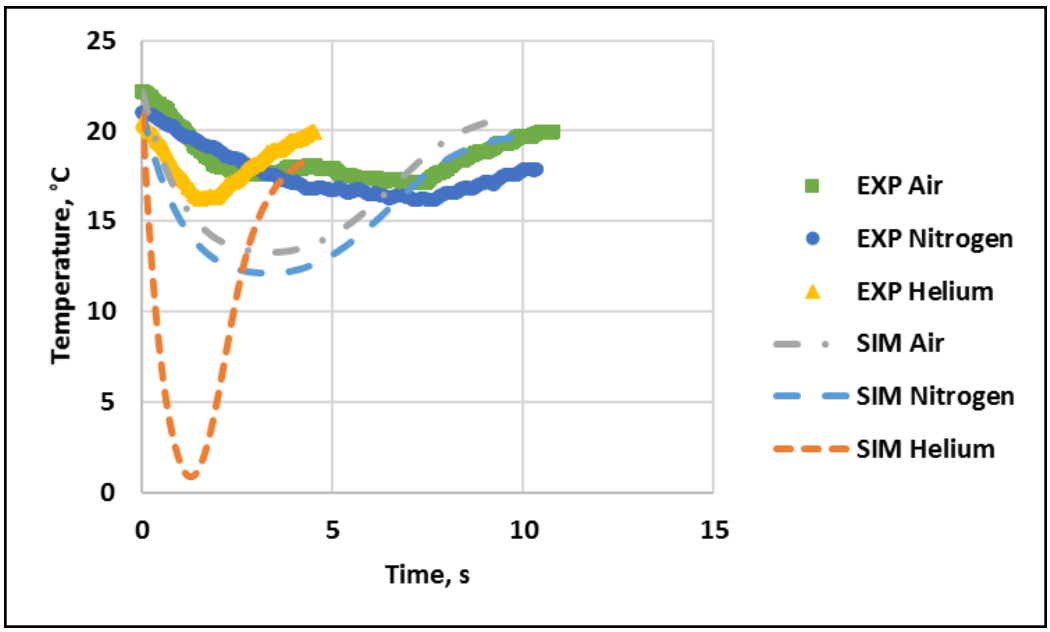

Figure 35. Temperature profiles in vessel 2 for the comparison of the behavior of different gases during depressurization

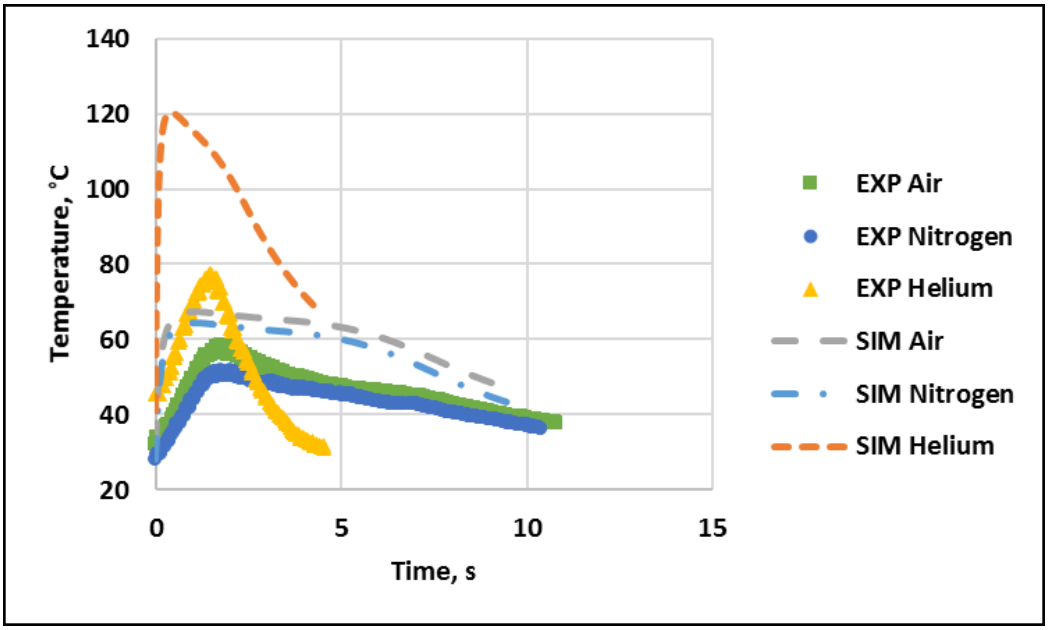

Figure 36. Temperature profiles in vessel 2 for the comparison of the behavior of different gases during depressurization

The temperature profiles for different gases can be observed in Figures 35 and 36. The profiles for air and nitrogen are similar due to the similarity of the gases. Nitrogen is a diatomic molecule whose molar heat capacity at constant pressure is similar to that of oxygen, which is also a diatomic molecule. Due to its lower value of the heat capacity, helium has more prominent temperature change in each vessel as compared to the other two gases. It can be observed from the plots that, although there are slight disagreements between the predicted temperature profile for nitrogen and air, and greatly exaggerated temperature profile for the helium gas, the simulator shows that it captures the trend with the assumptions used in the study for the simplicity of the model. The over-prediction of the temperature profile of the helium gas is possibly due to heat transfer coefficients used which were calibrated for the case of air, whereas the coefficients actually depend on the nature of the gas.

5.7 Impact of different compositions in a mixture of gases on depressurization

The vessel is filled with a mixture of air, nitrogen and helium gas at different composition where the final pressure is 15 bar. The vessel is then depressurized and vented to the catch-tank initially at 1 bar of air via 1/8-inch tube. Table 16 shows the initial conditions in each experiment performed.

Table 16. Initial conditions to study the effect of composition variation in a mixture of gas

Composition, mol % (N_2 : Air : He)	Vessel 1		Vessel 2	
	Pressure (bar)	Temperature (°C)	Pressure (bar)	Temperature (°C)
33.3 : 33.3 : 33.3 (equimolar)	15.04	23.67	0.98	31.83
53.3 : 33.3 : 13.3	15.10	23.86	1.00	31.63
13.3 : 33.3 : 53.3	15.00	22.96	1.01	36.17

The purpose of the study is to demonstrate how varying the composition affects the temperature and pressure in each vessel during the depressurization process. Another objective is to check whether the simulator is able to predict the impact seen in the experimental results.

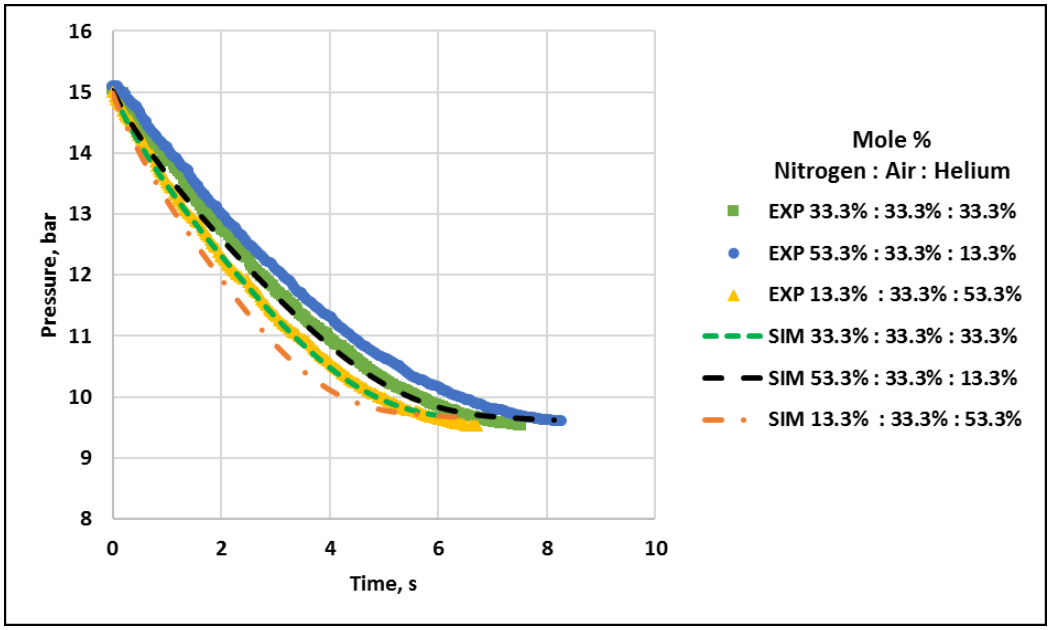

Figure 37. Pressure profiles in vessel 1 of different composition in a mixture of gases during depressurization

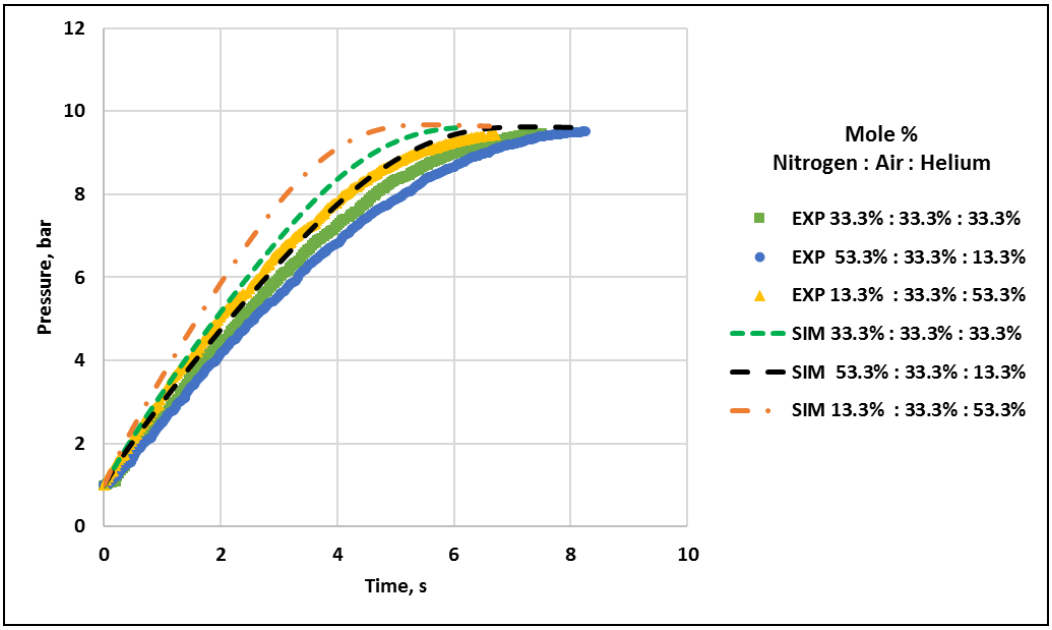

Figure 38. Pressure profiles in vessel 2 of different composition in a mixture of gases during depressurization

Figures 37 and 38 show the pressure profiles of three different compositions of the mixture depressurized from vessel 1. The impact of composition is found to be insignificant on the final pressure obtained from either the experiments or the simulations. It can be observed that the mixture with high composition of helium reaches equilibrium sooner as it behaves more like helium, which is a lighter gas as compared to the other two mixtures. Apart from capturing the trends, the simulator has also shown to predict the depressurization time and the equilibrium pressures correctly in each experiment.

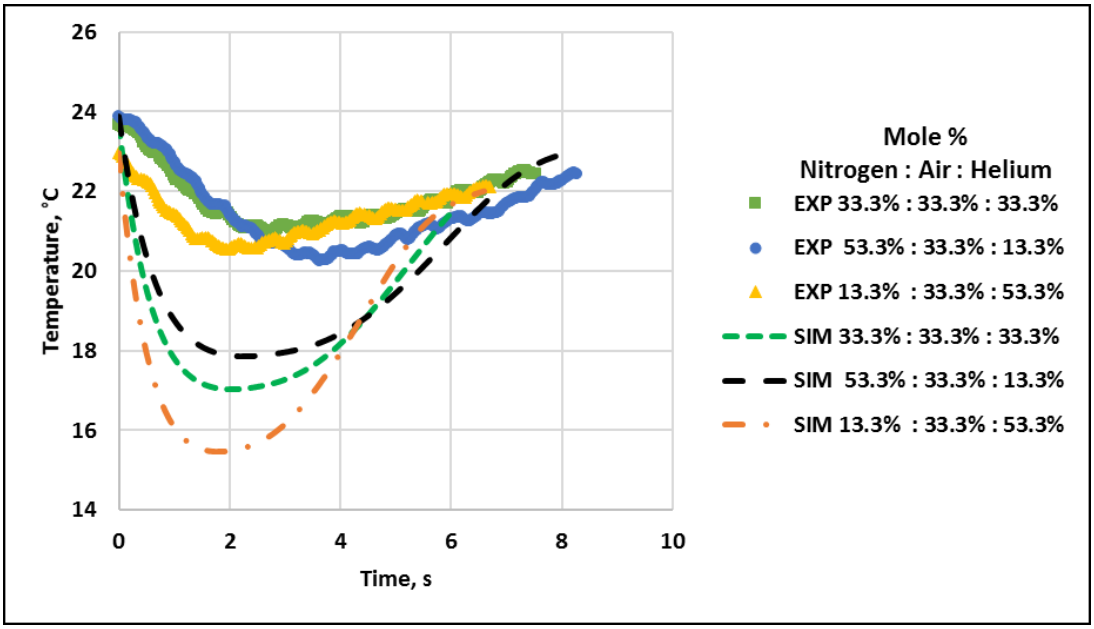

Figure 39. Temperature profiles in vessel 1 of different composition in a mixture of gases during depressurization

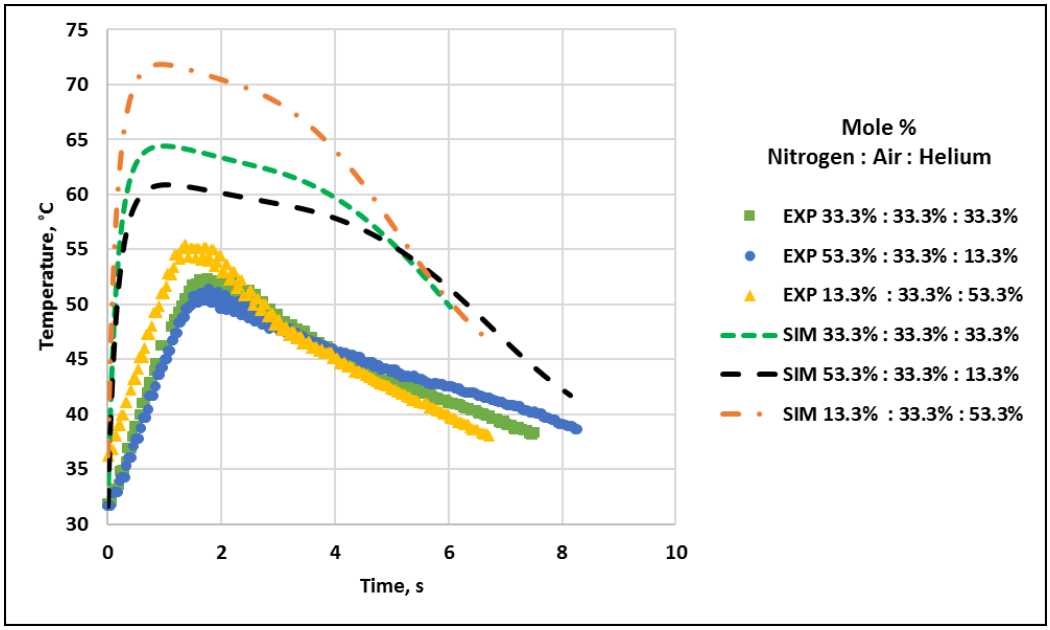

Figure 40. Temperature profiles in vessel 2 of different composition in a mixture of gases during depressurization

The temperature change is slightly higher for the mixture with higher composition of helium gas, as shown in Figures 39 and 40, because of it has lower heat capacity than the other two gases. Upon comparison of simulated and experimental results, it can be seen that the simulator over-predicts the temperature changes compared to the experimental data however the trends look similar. The large temperature changes predicted by the simulator are possibly due to the use of calibrated heat transfer coefficient for air. Since the gas is not just air anymore, the contribution from other gases to heat transfer also becomes important.

5.8 Impact of using different tube dimension for venting on depressurization

Figures 41-44 show the experiments conducted by varying the tube size used for venting the gas to the catch-tank. The experiments shown here includes air-filled vessel at 25 bar depressurized and vented to a catch-tank which is initially at 1 bar via two different tube sizes i.e. 1/8-inch and 1/16-inch stainless steel tube. For simulations, the value of discharge coefficient as shown in table 9 was recalibrated for the case of venting from a 1/16-inch tube. The initial temperatures for each experiment varying the tube size is given in Table 17.

Table 17. Initial conditions to study the effect different tube sizes for venting to catch-tank

Tube size	Vessel 1		Vessel 2	
	Pressure (bar)	Temperature (°C)	Pressure (bar)	Temperature (°C)
1/8-inch	25.06	22.12	1.00	32.35
1/16-inch	24.96	24.04	1.02	25.18

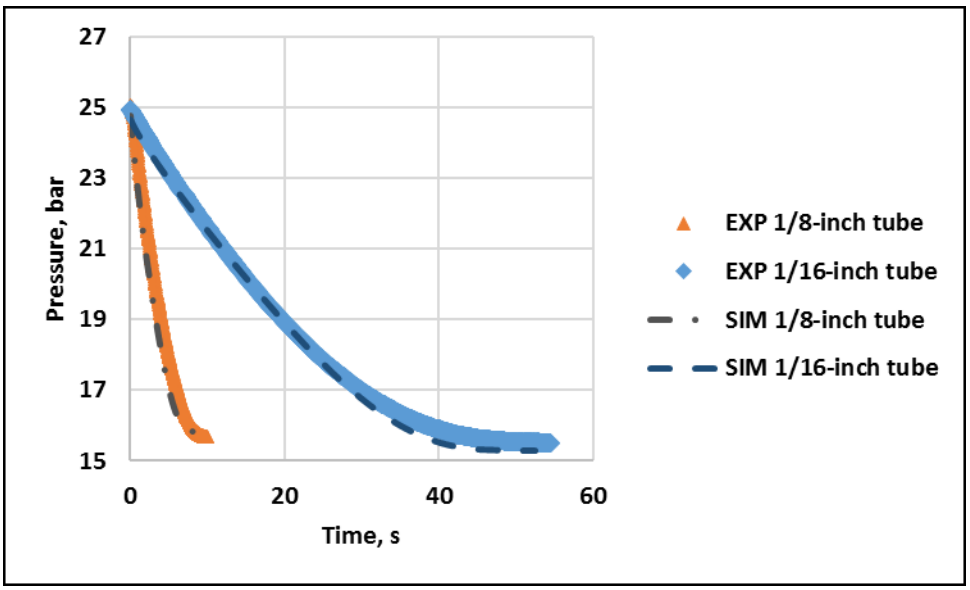

Figure 41. Pressure profiles in vessel 1 when varying tube dimensions used during depressurization

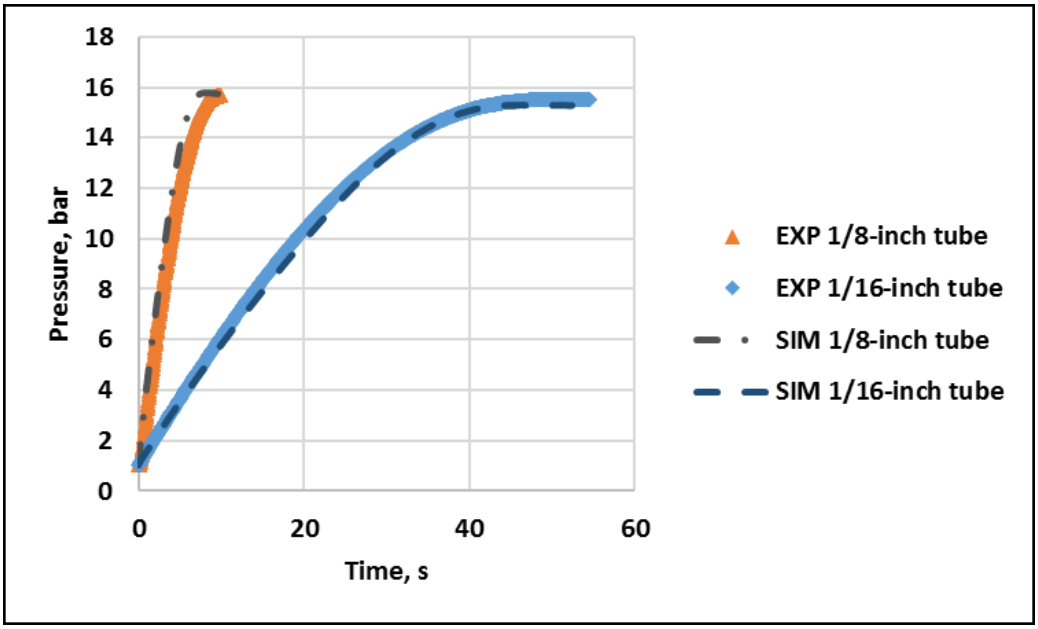

Figure 42. Pressure profiles in vessel 2 when varying tube dimensions used during depressurization

Figures 41 and 42 show that depressurization is greatly impacted by the reduction of the tube diameter, which leads to higher depressurization time. Symmetrical pressure profiles are observed and the simulation results are in good agreement with the experimental results.

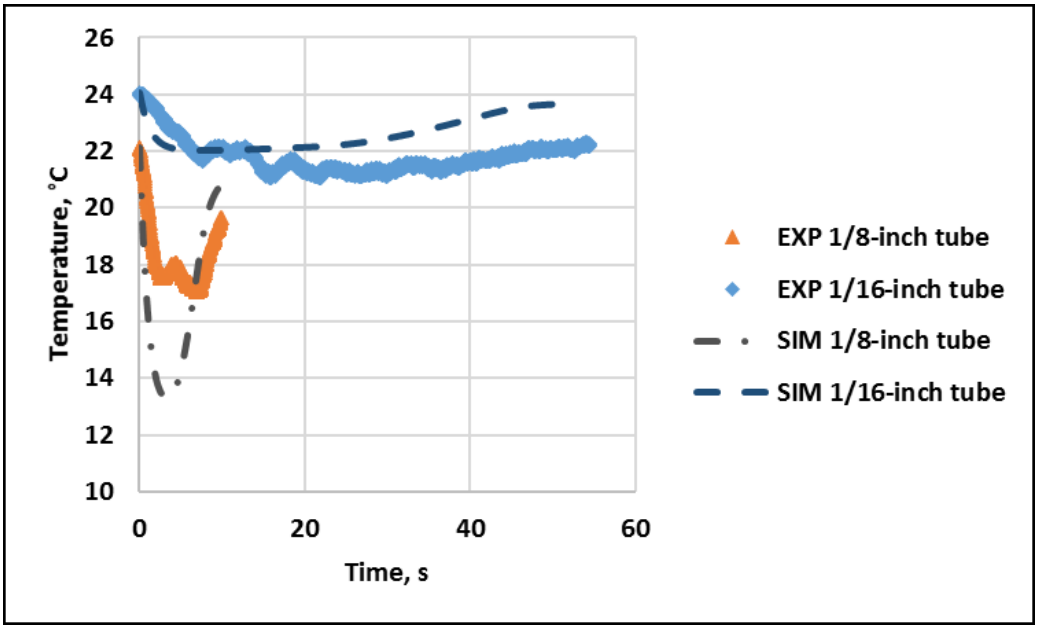

Figure 43. Temperature profiles in vessel 1 when varying tube dimensions used during depressurization

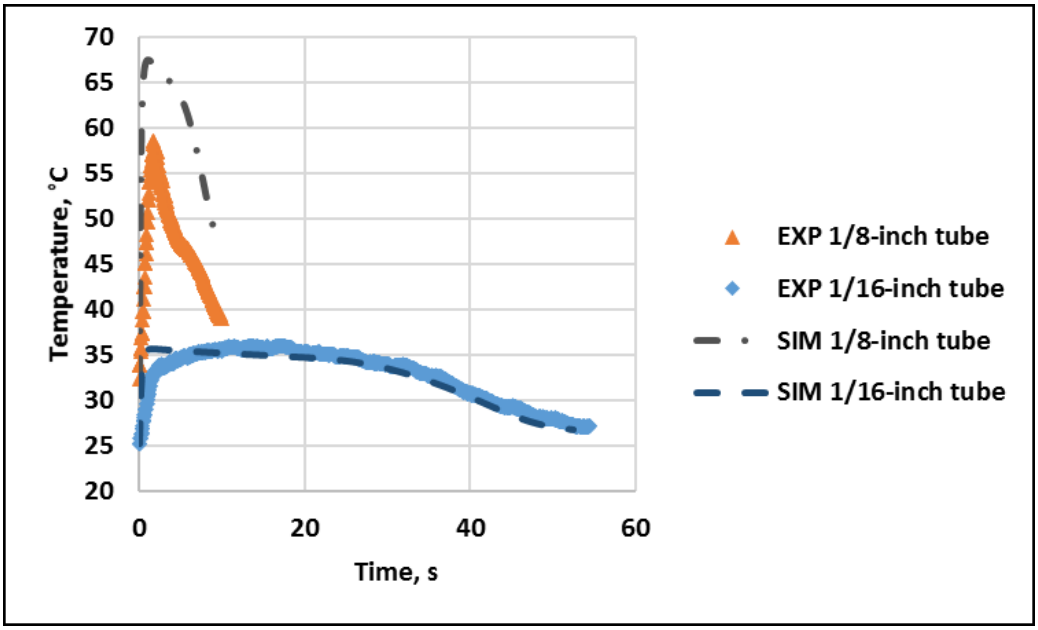

Figure 44. Temperature profiles in vessel 2 when varying tube dimensions used during depressurization

The temperature profiles of the smaller tube show significantly less change as compared to the larger tube for venting. This is because, when a smaller tube is used, the flow between the vessels is also reduced, increasing the time required to achieve equilibrium. The larger time for depressurization also allows for more heat transfer to take place with the walls of the vessel and hence the temperature change of the fluids in the vessels is less pronounced for the smaller tube than for the larger tube.

The experiments have also shown that time constant associated with the thermocouple plays an important role in the measurement of the temperature in each vessel. Since the flowrate through the 1/16-inch tube is much smaller than through the 1/8-inch tube, its impact can be seen on the temperature plots in which the change is less sudden and much smaller. Therefore, the data

obtained from 1/16-inch tube experiments are more reliable when using a thermocouple with higher value of response time. However, for the larger tube, the time constant results in a shift of the temperature data where the depressurization time is small, causing difficulty and raising uncertainty in the experiments.

The simulator shows excellent agreement with the experimental data for the smaller tube while over-predicts the temperature where the depressurization rate was higher. However, the trend of the temperature profile is correctly predicted.

6. CONCLUSION AND FUTURE WORK

An existing dynamic simulator capable of simulating leaks and venting from pressure vessel was extended to simulate the depressurization of a vessel vented to a catch-tank that receives the emergency discharge. The extension included incorporation of an algorithm to simulate multiple interconnected vessels at the same time-step while accounting for the heat transfer that takes place between the fluid and the vessel walls. The results were validated with another dynamic simulator called EMSO and experimental data which showed good potential in the prediction of the temperature, pressure and number of moles in each vessel during the depressurization process.

6.1 Conclusions

The simulations performed in this study show that the results are very sensitive to the values adopted for the discharge coefficient and the heat transfer coefficients. A higher value of the heat transfer coefficient results in lower change in temperature of the gas inside the vessel and vice versa. A significantly smaller discharge coefficient at the exit of vessel 1 found using the calibration technique suggests that the gas flow may encounter another discharge coefficient at the entrance of the vessel 2. Therefore, a combined effect of the discharge coefficient at the exit and entrance of the vessels results in a smaller value.

The simulations have shown that the molar masses and heat capacities of the gases affect the depressurization time and the temperature of the gas. A lighter gas flows with a relatively higher flowrate than a heavier gas, therefore reducing the depressurization time. Monoatomic and

diatomic gases have been used and both the experiments and the simulations indicated that monoatomic gases, which have lower heat capacities, undergo larger temperature changes than diatomic gases during analogous discharge processes.

The time constant associated with the thermocouples used in the experiments impacted the data collected by resulting in a shift of the data. In particular, the time constant represents substantial portion of the depressurization time for 1/8-inch tube experiments. The application of first order dynamics to the experimental temperature data provides a noisy inferred temperature inside each vessel which was smoothened by using a moving average technique. However, the inferred temperatures still show small fluctuations and peaks which indicate uncertainty in the corrected data. The comparison between 1/16-inch and 1/8-inch tube experiments shows that the former gives more reliable results because the depressurization time is longer and the flowrate is relatively smaller. The results of the 1/16-inch tube experiments exhibit no sudden changes and peaks in the temperature data and seem to be more reliable than the experimental results with the 1/8-inch tube Regarding the simulations, they closely follow the experimental trend for the 1/16-inch tube but do not predict the fluctuations and peaks measured with the 1/8-inch tube.

Finally, the results from the experimental study were used to validate the simulator, which showed good agreement with the pressure change during the depressurization of the vessel. Regarding temperature, it is able to capture the experimental trends but, in most cases, over-predicts the temperature change in each vessel, possibly as a result of using a constant and calibrated heat transfer coefficient for the case of depressurization of air-filled vessel at 10 bar.

6.2 Future work

The work in this thesis has been helpful in pointing out some issues one might have while studying the depressurization of interconnected vessels. Therefore, there is a room for improvement in the model and the experiments conducted to validate it, which may allow for better agreement between the experimental and simulation data.

The simulator currently lacks a model for the pipe that connects the process vessel and the catch-tank: the fluid is assumed to enter the catch-tank directly. However, it is important to calculate the expected pressure drop and heat generation due to friction in the pipe flow during the depressurization process. Moreover, the complexities of the heat transfer between the pipe and the fluid, and the two-phase flow through the pipe should be incorporated into the model for creating a generalized simulator that would be able to simulate both non-reacting and reacting cases in which phase change occurs.

In this work, a one-dimensional transient heat transfer model has been added to the simulator assuming that the vessels are insulated and that the heat transfer coefficients have constant values. However, if the vessel wall thickness is small, the heat transfer with the surroundings may become significant and important to account for in the model. Furthermore, the heat transfer coefficient depends on viscosity, density, heat capacity and thermal conductivity of the material, which are all temperature dependent properties [57]. As the temperature continuously changes during the depressurization, the heat transfer coefficients will change as well, which will influence the of heat transfer rate with the vessel walls and ultimately the predicted temperatures of the gas and the

vessel wall. Therefore, for future work, it is recommended to relax the assumption of thermally insulated vessels and add to simulator correlations to predict heat transfer coefficients. In addition, in case of a multiphase system, the current one-dimensional heat transfer model may not be sufficient and may require a two-dimensional heat transfer model because the heat transfer rate will be different for gases and liquids which may lead to a vertical temperature gradient within the vessel walls.

The experimental setup used in the study showed good potential for carrying out different depressurization experiments, however thermocouples with lower time constant, such as exposed butt welded 0.001 inch diameter, which has a time constant of 0.003 seconds, will reduce the uncertainty in the obtained experimental data [51]. The use of a thermocouple with a smaller response time would also avoid the need for applying a first order dynamics to the sensor (which can be assumed instantaneous), hence eliminating the uncertainty that results from the correction of the data. Furthermore, the use of multiple thermocouples inside the vessel at different positions can increase the confidence on the gas temperature data collected while also studying homogeneity and uniformity of the temperature of the gas inside each vessel. Lastly, temperature measurements within the walls of the vessel can provide a way for the validation of the wall temperatures calculated by the simulator during the depressurization and filling process.

The discharge coefficient varies as the ratio of the pressure in vessels changes with time and increases due to sonic flow, however the effect of sonic flow on discharge coefficient has not been accounted for in this study. It is recommended that future versions of the simulator include correlations for evaluating discharge coefficients.

The simulator is capable of handling a runaway reaction system with a reactor vessel connected to a catch-tank but this work was limited to non-reacting systems. In addition to aforementioned suggestions, the focus of future work should be on simulating a reactor (runaway reaction case) connected to a catch-tank for the sizing of the relief valve or the catch-tank using a similar methodology as described in this thesis for non-reacting fluids.

REFERENCES

[1] J. Barton, R. Rogers, Institution of Chemical Engineers (Great Britain), Chemical reaction hazards : a guide to safety, 2nd ed., Gulf Pub. Co., Houston, Texas, 1997.

[2] American Institute of Chemical Engineers. Center for Chemical Process Safety., Knovel (Firm), Guidelines for pressure relief and effluent handling systems, in, The Institute,, New York, N.Y., 1998, pp. xix, 538 p.

[3] American Institute of Chemical Engineers. Center for Chemical Process Safety., Knovel (Firm), Safe design and operation of process vents and emission control systems, in: CCPS concept book, Wiley-Interscience,, Hoboken, N.J., 2006, pp. xvi, 327 p.

[4] R. Kanes, A. Basha, L.N. Vechot, M. Castier, Simulation of venting and leaks from pressure vessels, J. Loss Prev. Process Ind., 40 (2016) 563-577.

[5] M. Castier, A. Basha, R. Kanes, L.N. Vechot, Discharge of Non-Reactive Fluids from Vessels, Braz. J. Chem. Eng., 34 (2017) 1149-1159.

[6] D.A. Crowl, J.F. Louvar, Chemical process safety : fundamentals with applications, 3rd ed., Prentice Hall, Upper Saddle River, NJ, 2011.

[7] S. Mannan, F.P. Lees, Lee's loss prevention in the process industries hazard identification, assessment, and control, in, Butterworth-Heinemann ;

Elsevier,, Boston

Amsterdam, 2012, pp. 1 online resource (3 volumes in 1 (xli, 3642 pages)).

[8] J. Lenclud, J.E.S. Venart, Single and two-phase discharge from a pressurized vessel, Rev. Gen. Therm., 35 (1996) 503-516.

[9] J.L. Woodward, K.S. Mudan, Liquid and gas discharge rates through holes in process vessels, J. Loss Prev. Process Ind., 4 (1991) 161-165.

[10] A.P. Institute, API Standard 520: Sizing, selection, and installation of pressure-relieving devices in refineries, American Petroleum Institute, 2008.

[11] J.C. Leung, M. Epstein, A Generalized Critical Flow Model for Nonideal Gases, AIChE J., 34 (1988) 1568-1572.

[12] J.C. Leung, Venting of Runaway Reactions with Gas Generation, AIChE J., 38 (1992) 723-732.

[13] J.C. Leung, A theory on the discharge coefficient for safety relief valve, J. Loss Prev. Process Ind., 17 (2004) 301-313.

[14] R. Diener, A. Schmidt, Sizing of throttling device for gas/liquid two-phase flow - Part 1: Safety valves, Process Saf. Prog., 23 (2004) 335-344.

[15] W.R. Byrnes, F.E. Ruccia, R.C. Reid, Rapid Depressurization of Gas Storage Cylinder, Ind. Eng. Chem. Process Des. Dev., 3 (1964) 206-209.

[16] C.S. Landram, Heat-Transfer during Vessel Discharge - Mean and Fluctuating Gas Temperature, J HEAT TRANS-T ASME, 95 (1973) 101-106.

[17] A. Haque, S. Richarson, G. Saville, G. Chamberlain, Rapid Depressurization of Pressure-Vessels, J. Loss Prev. Process Ind., 3 (1990) 4-7.

[18] M.A. Haque, S.M. Richardson, G. Saville, Blowdown of Pressure-Vessels .1. Computer-Model, Process Saf. Environ. Prot., 70 (1992) 3-9.

[19] M.A. Haque, S.M. Richardson, G. Saville, G. Chamberlain, L. Shirvill, Blowdown of Pressure-Vessels .2. Experimental Validation of Computer-Model and Case-Studies, Process Saf. Environ. Prot., 70 (1992) 10-17.

[20] A.N. Skouloudis, K. Bell, H.M. Kottowski, Venting of Vessels Containing Reacting Fluids - a Parametric Study with Safire and Deers, J. Loss Prev. Process Ind., 3 (1990) 13-16.

[21] M. A. Grolmes, J. C. Leung, Code Method for Evaluating Integrated Relief Phenomena, 1985.

[22] K.H. H., Analysis of diers venting tests: Validation of a tool for sizing emergency relief systems for runaway chemical reactions, Plant/Oper. Prog., 5 (1986) 1-10.

[23] L. Friedel, H.G. Schecker, G. Wehmeier, Recalculation of the Pressure Behavior in the Reactor and in the Catchtank during Emergency Depressurization, J. Loss Prev. Process Ind., 5 (1992) 229-233.

[24] J.L. Xia, B.L. Smith, G. Yadigaroglu, A Simplified Model for Depressurization of Gas-Filled Pressure-Vessels, Int. Commun. Heat Mass Transfer, 20 (1993) 653-664.

[25] H.K. Onnes, Expression of the equation of state of gases and liquids by means of series, P K Akad Wet-Amsterd, 4 (1902) 125-147.

[26] H. Mahgerefteh, S.M.A. Wong, A numerical blowdown simulation incorporating cubic equations of state, Comput. Chem. Eng., 23 (1999) 1309-1317.

[27] T.J. Snee, L. Cusco, Pilot-scale evaluation of the inhibition of exothermic runaway, Process Saf. Environ. Prot., 83 (2005) 135-144.

[28] G. Berge, Verification of VessFire, in, Petrell, 2009.

[29] C.N. Ranong, S. Maus, J. Hapke, G. Fieg, D. Wenger, Approach for the Determination of Heat Transfer Coefficients for Filling Processes of Pressure Vessels With Compressed Gaseous Media, Heat Transfer Eng., 32 (2011) 127-132.

[30] W.S. Winters, G.H. Evans, S.F. Rice, R. Greif, An experimental and theoretical study of heat and mass transfer during the venting of gas from pressure vessels, Int. J. Heat Mass Transfer, 55 (2012) 8-18.

[31] V. D'Alessandro, G. Giacchetta, M. Leporini, B. Marchetti, A. Terenzi, Modelling blowdown of pressure vessels containing two-phase hydrocarbons mixtures with the partial phase equilibrium approach, Chem. Eng. Sci., 126 (2015) 719-729.

[32] B. Fischer, S. Biswas, Validation of BLOWDOWN™ Technology in V9 of Aspen HYSYS®, in, aspentech, 2016.

[33] K. Kim, J. Seo, S. Hwang, Y. Lee, Y. Moon, Dynamic Modeling & Analysis of Vapor Phase Blowdown of Depressurized Vessel, Korean Chem Eng Res, 54 (2016) 350-359.

[34] D. Peng, D.B. Robinson, A New Two-Constant Equation of State, Ind. Eng. Chem. Fundam., 15 (1976) 59-64.

[35] G. Soave, Equilibrium Constants from a Modified Redlich-Kwong Equation of State, Chem. Eng. Sci., 27 (1972) 1197-&.

[36] A. Park, Y. Ko, S. Ryu, Y. Lim, Numerical modeling of rapid depressurization of a pressure vessel containing two-phase hydrocarbon mixture, Process Saf. Environ. Prot., 113 (2018) 343-356.

[37] F.M. Goncalves, M. Castier, O.Q.F. Araujo, Dynamic simulation of flash drums using rigorous physical property calculations, Braz. J. Chem. Eng., 24 (2007) 277-286.

[38] M. Castier, Solution of the isochoric-isoenergetic flash problem by direct entropy maximization, Fluid Phase Equilib., 276 (2009) 7-17.

[39] M. Castier, Dynamic simulation of fluids in vessels via entropy maximization, J. Ind. Eng. Chem., 16 (2010) 122-129.

[40] M. Castier, Thermodynamic speed of sound in multiphase systems, Fluid Phase Equilibr, 306 (2011) 204-211.

[41] N. Saha, R. Al-Muhannadi, A. Al-Mohannadi, L.N. Vechot, M. Castier, Is it the time to say bye to the phi-factor?, Process Saf. Environ. Prot., 113 (2018) 193-203.

[42] S. Selmar-Olsen, Pressure Relief and Two-Phase Flow, in, 1992.

[43] R.D.P. Soares, A.R. Secchi, EMSO: A new environment for modelling, simulation and optimisation, European Symposium on Computer Aided Process Engineering - 13, 14 (2003) 947-952.

[44] R.B. Bird, W.E. Stewart, E.N. Lightfoot, Transport Phenomena, Wiley, 2007.

[45] S. Linge, H.P. Langtangen, Solving Partial Differential Equations, in: Programming for Computations - Python, Springer, Cham, 2016.

[46] M.S. Peters, K.D. Timmerhaus, R.E. West, Plant Design and Economics for Chemical Engineers, McGraw-Hill Education, 2003.

[47] R. Kanes, Modeling the Behavior of a Vessel under Runaway Conditions, in, Texas A & M University, 2015.

[48] A. Basha, Rigorous Simulation of Accidental Leaks from High-Pressure Storage Vessels, in, Texas A & M University, 2014.

[49] Overview, Low Thermal Inertia (Low Phi-Factor) Accelerating Rate Calorimeter (ARC) | Phi-TEC II | HEL Group. https://www.helgroup.com/reactor-systems/thermal-hazards-and-calorimetry/phitec-ii/.

[50] Series 4600 Pressure Vessel Systems, 1 & 2 L, Parr Instrument Company. https://www.parrinst.com/products/non-stirred-pressure-vessels/series-4600/.

[51] Thermocouple Response Time, Omega Engineering. https://www.omega.com/techref/ThermocoupleResponseTime.html.

[52] K. Kalantar-zadeh, Sensors an introductory course, in, Springer,, New York, 2013, pp. 1 online resource.

[53] S.b.A. Design Institute for Physical Properties, DIPPR Project 801 - Full Version, in, Design Institute for Physical Property Research/AIChE.

[54] J.J. Valencia, P.N. Quested, Thermophysical Properties, in: ASM Handbook Volume 15: Casting, ASM International, 2008, pp. 468-481.

[55] J.R. Couper, Chemical process equipment : selection and design, Rev. 2nd ed., Elsevier Butterworth-Heinemann, London, 2010.

[56] E.E. Ludwig, Applied process design for chemical and petrochemical plants, 3rd ed., Gulf Pub. Co., Houston, 1995.

[57] J.P. Holman, Heat transfer, 9th ed., McGraw-Hill, New York, 2002.